Department of Neuroscience Faculty Papers

Department of Neuroscience

8-8-2021

# CalDAG-GEFI mediates striatal cholinergic modulation of dendritic excitability, synaptic plasticity and psychomotor behaviors.

Jill R. Crittenden

Shenyu Zhai

Magdalena Sauvage

Takashi Kitsukawa

Eric Burguière

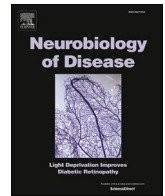*See next page for additional authors*

## Authors

Jill R. Crittenden, Shenyu Zhai, Magdalena Sauvage, Takashi Kitsukawa, Eric Burguière, Morgane Thomsen, Hui Zhang, Cinzia Costa, Giuseppina Martella, Veronica Ghiglieri, Barbara Picconi, Karen A. Pescatore, Ellen M. Unterwald, Walker S. Jackson, David E. Housman, S. Barak Caine, David Sulzer, Paolo Calabresi, Anne C. Smith, D. James Surmeier, and Ann M. Graybiel

# CalDAG-GEFI mediates striatal cholinergic modulation of dendritic excitability, synaptic plasticity and psychomotor behaviors

Jill R. Crittenden [a,b,1], Shenyu Zhai [c,1], Magdalena Sauvage [a,d], Takashi Kitsukawa [e], Eric Burguière [a,f], Morgane Thomsen [g,o], Hui Zhang [h,i], Cinzia Costa [j], Giuseppina Martella [k], Veronica Ghiglieri [l], Barbara Picconi [m], Karen A. Pescatore [n], Ellen M. Unterwald [n], Walker S. Jackson [o], David E. Housman [b], S. Barak Caine [p], David Sulzer [h], Paolo Calabresi [q,r], Anne C. Smith [s], D. James Surmeier [c], Ann M. Graybiel [a,*,2]

[a] McGovern Institute for Brain Research and Dept. of Brain and Cognitive Sciences, MIT, Cambridge, MA 02139, USA
[b] Koch Institute for Integrative Cancer Research, MIT, Cambridge, MA 02139, USA
[c] Department of Physiology, Feinberg School of Medicine, Northwestern University, Chicago, IL 60611, USA
[d] Leibniz Institute for Neurobiology, Functional Architecture of Memory Dept., Magdeburg, Germany
[e] Graduate School of Frontier Biosciences, Osaka University, Osaka, Japan
[f] Brain and Spine Institute (ICM), CNRS UMR 7225, INSERM U 1127, UPMC-P6 UMR S, 1127, Hôpital de la Pitié-Salpêtrière, 47 boulevard de l'hôpital, Paris, France
[g] Laboratory of Neuropsychiatry, Psychiatric Centre Copenhagen and University, DK-2100, Copenhagen, Denmark
[h] Departments of Psychiatry, Pharmacology, Neurology, Columbia University, New York State Psychiatric Institute, New York, NY 10032, USA
[i] Department of Neuroscience, Thomas Jefferson University, Philadelphia, PA 19107, USA
[j] Neurological Clinic, Department of Medicine, Hospital Santa Maria della misericordia, University of Perugia, 06100 Perugia, Italy
[k] Neurophysiology and Plasticity, IRCCS Fondazione Santa Lucia, Via del Fosso di Fiorano 64, 00143 Rome, Italy
[l] San Raffaele University, 00166 Rome, Italy
[m] IRCCS San Raffaele Pisana, Rome 00166, Italy
[n] Department of Pharmacology and Center for Substance Abuse Research, Temple University School of Medicine, Philadelphia, PA 19140, USA
[o] Wallenberg Center for Molecular Medicine, Department of Clinical and Experimental Medicine, Linköping University, 581 83 Linköping, Sweden
[p] Basic Neuroscience Division, McLean Hospital/Harvard Medical School, Belmont, MA 02478, USA
[q] Neurological Clinic, Fondazione Policlinico Universitario Agostino Gemelli IRCCS, 00168 Rome, Italy
[r] Department of Neuroscience, Faculty of Medicine, Università Cattolica del "Sacro Cuore", 00168 Rome, Italy
[s] Evelyn F. McKnight Brain Institute, University of Arizona, Tucson, AZ 85724, USA

## ARTICLE INFO

## ABSTRACT

CalDAG-GEFI (CDGI) is a protein highly enriched in the striatum, particularly in the principal spiny projection neurons (SPNs). CDGI is strongly down-regulated in two hyperkinetic conditions related to striatal dysfunction: Huntington's disease and levodopa-induced dyskinesia in Parkinson's disease. We demonstrate that genetic deletion of CDGI in mice disrupts dendritic, but not somatic, M1 muscarinic receptors (M1Rs) signaling in indirect pathway SPNs. Loss of CDGI reduced temporal integration of excitatory postsynaptic potentials at dendritic glutamatergic synapses and impaired the induction of activity-dependent long-term potentiation. CDGI deletion selectively increased psychostimulant-induced repetitive behaviors, disrupted sequence learning, and eliminated M1R blockade of cocaine self-administration. These findings place CDGI as a major, but previously unrecognized, mediator of cholinergic signaling in the striatum. The effects of CDGI deletion on the self-administration of drugs of abuse and its marked alterations in hyperkinetic extrapyramidal disorders highlight CDGI's therapeutic potential.

---

* Corresponding author at: McGovern Institute for Brain Research and Dept. of Brain and Cognitive Sciences, MIT, Cambridge, MA 02139, USA.
  *E-mail address:* graybiel@mit.edu (A.M. Graybiel).
[1] Co-first authors
[2] Lead Contact.

## 1. Introduction

CalDAG-GEFI (CDGI) is a striatum-enriched signaling molecule that is allosterically activated by $Ca^{2+}$ to stimulate the small GTPase Rap1 (Crittenden et al., 2004; Kawasaki et al., 1998; Toki et al., 2001). Working through Rap1, CDGI has been shown to modulate multiple pathways in non-neuronal cell types *in vivo*, including integrin-adhesion to surface ligands, vesicle release, and activity of the mitogen-activated kinases (MAPKs), extracellular signal-activated kinase (ERK) and p38-MAPK (Crittenden et al., 2004; Crittenden et al., 2019; Guo et al., 2001; ; Kawasaki et al., 1998; Stefanini and Bergmeier, 2010; ). Given that Rap1 signaling cascades are linked to a variety of downstream effectors that can impact ion channels, transcription factors, cell adhesion, cell death, neuroplasticity and more (Impey et al., 1999; York et al., 1998; Kosuru and Chrzanowska, 2020; Huang et al., 2004; Takeda and Ichijo, 2002), CDGI is in a position, within select cells of expression, to modulate a wide array of functions.

One potential clue to the upstream signaling that activates neuronal CDGI is its robust expression in spiny projection neurons (SPNs) of the matrix compartment of the striatum (Kawasaki et al., 1998). The matrix compartment is highly enriched with molecules related to cholinergic signaling, of which choline acetyltransferase and acetylcholinesterase are examples (Graybiel et al., 1986; Graybiel and Ragsdale, 1978). Moreover, in PC12 cell cultures, M1 muscarinic receptors (M1Rs) signal through CDGI, Rap1 and ERK (Guo et al., 2001). This further link to the cholinergic system raised the question of whether this signaling would hold for the SPNs. Like CDGI (Toki et al., 2001), M1Rs are expressed by both indirect pathway SPNs (iSPNs) and direct pathway SPNs (dSPNs) in the matrix compartment (Bernard et al., 1992; Hersch et al., 1994; Yan et al., 2001).

Strong further clues about the neurological functions of CDGI come from work related to clinical signs of extrapyramidal disorders. CDGI is early on and markedly down-regulated in the striatum in Huntington's disease (HD) and in rodent HD models (Crittenden et al., 2010; Desplats et al., 2006; Kuhn et al., 2007; Luthi-Carter et al., 2002). In a mimic of this situation, knock-down of CDGI in cultured striatal brain slices expressing a mutant fragment of huntingtin was found to rescue the HD model cellular phenotype in that it fully prevented the neurodegeneration that is normally caused by mutant huntingtin (Crittenden et al., 2010). CDGI was also found to be severely down-regulated in the 6-hydroxydopamine lesion model of Parkinson's disease in response to levodopa treatment, and the CDGI depletion was positively correlated with the severity of levodopa-induced dyskinesia (LID) (Crittenden et al., 2009). Thus, in two hyperkinetic disorders with strong striatal links—HD and LID—CDGI appears to be strongly dysregulated. In both of these disorders, hypoactivity of matrix iSPNs is thought to be one factor causally related to the behavioral deficits (Albin et al., 1989; Alcacer et al., 2017).

To test directly the striatal function of CDGI, we generated two lines of mice with deletions in the gene encoding CDGI: one in which the deletion was constitutive and global, and another in which deletion was limited to postnatal striatum. The constitutive CDGI knockout line was crossed with mice in which either iSPNs or dSPNs expressed a fluorescent marker (Gong et al., 2003). In these mice, the impact of CDGI deletion was examined in identified dSPNs or iSPNs. We found that CDGI has selective effects on dendritic M1R function in iSPNs, and that it is required for long-term synaptic potentiation in these cells. We further found that deletion of CDGI produces deficits in motor sequence learning and abnormalities in responses to psychomotor stimulant treatment, and that the deletion of CDGI prevents the capacity for M1R agonist treatment to block self-administration of cocaine. We propose CDGI to be a major modulator of striatal function by virtue of its essential position in M1R cholinergic receptor signaling.

## 2. Results

### 2.1. CDGI deletion did not produce generalized brain pathology or baseline behavioral deficits

To achieve constitutive knockout of CDGI, we engineered a deletion near the 5′ end of *CDGI* (aka *RasGRP2*) that resulted in a nonsense mutation (stop codon) (Fig. S1A). In brain tissue from mice that were homozygous for this mutation, the deleted exons were not detected in mRNA assays, and CDGI protein expression was lost (Figs. 1A-F and S1B-D,G). Expression of *CalDAG-GEFII* (aka *RasGRP*) mRNA was unchanged in CDGI knockout mice (Fig. S1H). CDGI is broadly expressed in the brain during prenatal development and, in the adult, is expressed at lower levels in some brain regions outside the striatum, including the cerebral cortex (Fig. 1A) (Crittenden et al., 2010; Kawasaki et al., 1998; Toki et al., 2001). To examine more specifically the function of striatal CDGI in the adult, we generated mice in which *CDGI* was floxed (Fig. S1A) and crossed them to D1-YAC Cre mice in which Cre recombinase was expressed after birth in the majority of SPNs (Lemberger et al., 2007) (Figs. 1G and S1E,F). The D1-YAC Cre line is reported to drive postnatal deletion in most SPNs that express the D1 dopamine (DA) receptor, and many that express the D2 receptor, with lesser activity in the cerebral cortex, cerebellum and other brain regions (Lemberger et al., 2007; Monory et al., 2007). Consistent with this account, we found that CDGI$^{flox/flox}$Cre(+) mice had normal CDGI expression in the striatum and olfactory tubercle at birth that gradually declined so that all striatal expression appeared to be gone by adulthood, but with maintained expression in the cerebral cortex (Figs. 1G and S1E,F).

Both constitutive and conditional CDGI knockout mice were fertile and displayed no obvious behavioral changes or abnormalities in brain structure. Neural exams of the constitutive CDGI knockouts showed normal gross brain anatomy (Fig. S2A), normal DA receptor binding in the striatum (Fig. S2B and Table S1), normal expression of striatal protein markers (Fig. S2C), normal transcriptome-wide striatal mRNA expression levels (Table S2) and normal levels of total striatal amino acids and biogenic amines (Tables S3 and S4). There were no differences between CDGI knockouts and sibling controls in adult weight, daily chow consumption (Fig. S2D), rotarod motor coordination (Fig. S2E), open-field behavior (Fig. S2F), olfactory acuity (Fig. S2G), responses on a SHIRPA neurological exam (Rogers et al., 1997) (Table S5), learned helplessness (Fig. S2H), marble-burying behavior (Fig. S2I), cue- or context-paired fear conditioning (Fig. S2J,K) or social recognition memory (Fig. S2L). Automated home-cage monitoring of behaviors showed no detectable differences between wildtype and CDGI knockout mice (Fig. S2M).

### 2.2. CDGI was not necessary for M1R modulation of SPN somatic excitability

To characterize the effects of CDGI deletion in identified iSPNs and dSPNs, *ex vivo* parasagittal brain slices were prepared from constitutive CDGI knockout mice crossed with either *Drd2*-EGFP or *Drd1*-tdTomato reporter lines, and patch clamp recordings were made from visually identified neurons (Figs. 2A,B). Recordings were made from the dorsolateral striatum where CDGI-poor striosomes were scarce (Fig. 1E) (Crittenden et al., 2016). In recordings from wildtype SPNs, M1R activation promotes closing of Kv7 (KCNQ) potassium channels in the perisomatic region by depleting the plasma membrane lipid, phosphatidylinositol 4,5-bisphosphate (PIP$_2$). Closing of Kv7 K$^+$ channels increases somatic membrane resistance near spike threshold, resulting in increased somatic excitability (Shen et al., 2005). To determine whether CDGI participates in this modulation, we measured the spiking evoked by somatic current injection and its modulation by bath application of the muscarinic receptor agonist, oxotremorine-M (Oxo-M, 10 μM), using whole-cell recordings of iSPNs and dSPNs in *ex vivo* slices from CDGI knockout and wildtype mice. Consistent with
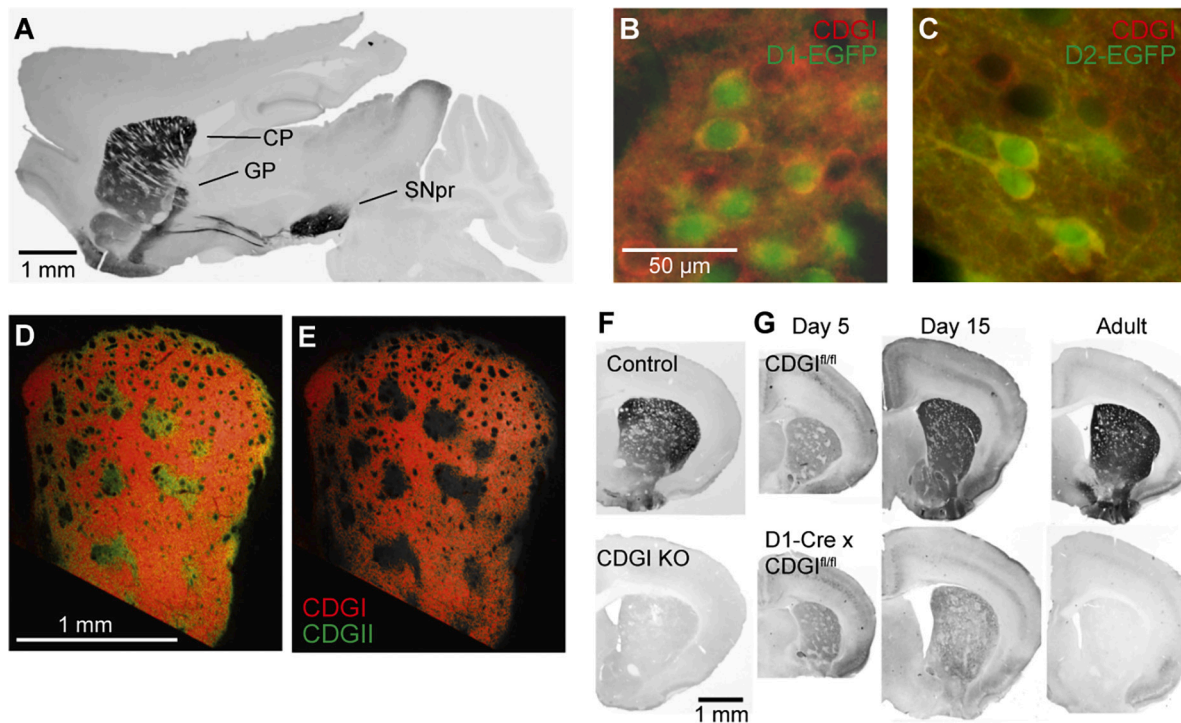
**Fig. 1.** Generation of CDGI global knockout and conditional knockout mice. (A) CDGI immunostaining in sagittal section through mouse brain showing expression in direct and indirect striatal output projections from the caudoputamen (CP) to, respectively, the substantia nigra pars reticulata (SNpr) and the external globus pallidus (GP). (B, C) CDGI immunofluorescence (red) shows co-expression in cell soma (yellow) with green fluorescent protein (EGFP) in transgenic mice that express EGFP in D1 direct pathway (B) or D2 indirect pathway (C) neurons. (D, E) CDGI (red) enriched in matrix relative to striosomes, shown in transverse mouse striatal section co-labeled for the striosomal marker CalDAG-GEFII (CDGII, green, shown in (D)). (F) CDGI immunoreactivity (black) in control (top) and global knockout (bottom) coronal mouse brain hemisection. (G) CDGI expression is lost postnatally in conditional CDGI$^{flox/flox}$ mice that carry a D1-yeast artificial chromosome (YAC) driving Cre expression (bottom) but not in CDGI$^{flox/flox}$ control mice (top). (For interpretation of the references to colour in this figure legend, the reader is referred to the web version of this article.)

previous observations (Shen et al., 2005), in both iSPNs and dSPNs from wildtype mice, Oxo-M produced a leftward shift in the relationship between intrasomatic current injection and spiking: less current was required to produce the same level of spiking across the full range of spiking rates (Figs. 2C,D,F,G). This modulation was intact in CDGI-deficient iSPNs and dSPNs (Figs. 2C,E,F,H).

### 2.3. CDGI was necessary for M1R-mediated modulation of iSPN dendritic excitability

In iSPNs (but not in dSPNs), M1R activation enhances dendritic excitability and the summation of excitatory post-synaptic potentials (EPSPs). This effect is accomplished by decreasing the opening of dendritic Kir2.3 potassium channels (Shen et al., 2007). We tested for the involvement of CDGI in this modulation of dendritic excitability by asking whether M1R signaling enhanced temporal summation in iSPNs from CDGI knockout mice. We stimulated corticostriatal glutamatergic axons (five pulses at 40 Hz) while monitoring somatic voltage in whole cell recordings of iSPNs (Fig. 2I). As expected, in iSPNs of wildtype mice, bath application of Oxo-M (10 μM) significantly increased dendritic EPSP summation, as estimated by the ratio of the fifth to the first EPSP amplitudes (EPSP5/EPSP1, Fig. 2J), and slowed the EPSP decay kinetics (Fig. 2K). The Oxo-M modulation was prevented by application of the M1R-specific antagonist VU0255035 (5 μM) (Sheffler et al., 2009) (Figs. 2I-K). In iSPNs from CDGI knockouts, by contrast, Oxo-M did not significantly affect the dendritic integration of glutamatergic EPSPs (Figs. 2I-K). These findings demonstrate that CDGI is necessary for the dendritic M1R-mediated modulation of Kir2 K$^+$ channels in iSPNs, in contrast to its lack of influence on the M1R modulation of somatic excitability.

### 2.4. CDGI mediated the M1R modulation of long-term potentiation in iSPNs

Given its dendritic function, we asked whether CDGI signaling might also be involved in long-term synaptic plasticity (Crittenden et al., 2019). A transient suppression of M1R signaling has been implicated in the induction of long-term depression (LTD) in SPNs (Wang et al., 2006), but its role in long-term synaptic potentiation (LTP) of glutamatergic synapses is controversial. An early report suggested that M1R signaling was necessary for LTP induction at corticostriatal synapses in both classes of SPN (Calabresi et al., 1999). However, recent work has shown that in dSPNs dendritic M4 muscarinic receptors blunt LTP induction (Hernandez-Flores et al., 2015; Shen et al., 2015), raising doubts about the potential role of M1Rs in dSPNs. To address this issue, we first recorded synaptic responses in wildtype iSPNs using a K$^+$-based internal solution before and after four bouts of high frequency stimulation (HFS; 100 Hz for 1 s) of glutamatergic axons with coincident intracellular depolarizing current pulse (1–2 nA for 1 s). This protocol induced a robust LTP in iSPNs that was blocked by the muscarinic receptor antagonist, scopolamine (10 μM) (Fig. 3A). In dSPNs, this HFS protocol did not produce LTP with normal extracellular Mg$^{2+}$ (1 mM) (Fig. 3C). However, when the extracellular Mg$^{2+}$ concentration was lowered to nominally zero, this protocol did induce LTP in dSPNs (Fig. 3C) (Calabresi et al., 1992a). However, in contrast to the LTP in iSPNs, antagonizing muscarinic receptors did not significantly affect the LTP in dSPNs (Fig. 3D). Next, we repeated these experiments in CDGI knockout mice. In dSPNs lacking CDGI, LTP induction was not significantly different from that seen in wildtype dSPNs (Fig. 3D). By contrast, in iSPNs lacking CDGI, LTP induction was significantly reduced, suggesting that CDGI signaling was critical to the dendritic signaling underlying LTP (Fig. 3B).
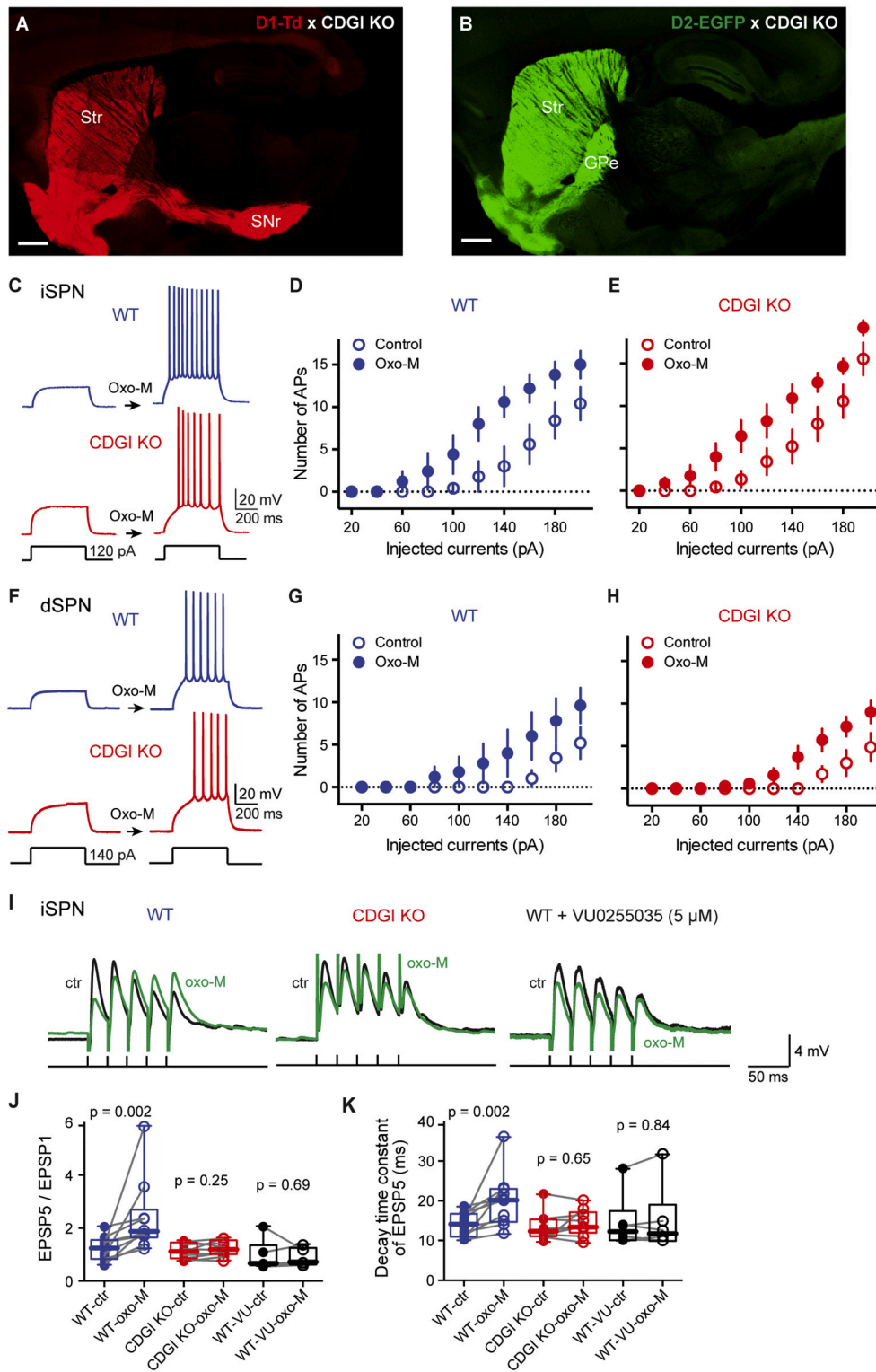
**Fig. 2.** CDGI mediates the M1R modulation of dendritic excitability but not the M1R modulation of somatic excitability. (A, B) Sagittal sections through the brains of CDGI knockout mice in which the direct pathway was visualized (red) in D1-tdTomato x CDGI knockout mice (A) and the indirect pathway was visualized (green) in D2-EGFP x CDGI knockout mice (B). (C) Sample somatic voltage changes evoked by 120 pA current injections in iSPNs from wildtype (WT, blue) and CDGI knockout (KO, red) mice before and after bath application of Oxo-M (10 µM). (D, E) Current-response curves of iSPNs from WT (D, $n = 5$ cells from 3 mice) and CDGI KO (E, $n = 7$ cells from 4 mice) mice. Somatic excitability of iSPNs was similarly enhanced by Oxo-M in WT and CDGI KO mice. Error bars show standard error of the mean (SEM). (F) Sample somatic recordings in response to 140 pA current injections in dSPNs from WT (blue) and CDGI KO (red) mice before and after bath application of Oxo-M (10 µM). (G, H) Current-response curves of dSPNs from WT (G, $n = 5$ cells from 3 mice) and CDGI KO (H, $n = 7$ cells from 3 mice) mice. (I) Trains of five EPSPs were evoked by stimulation of glutamatergic afferent fibers at 40 Hz. Oxo-M (10 µM) increased EPSP summation in iSPNs of WT mice, but not in CDGI KO mice or when M1Rs were blocked by M1R antagonist VU0255035 (5 µM) in WT mice. (J) Box plot showing the effect of Oxo-M on synaptic summation. The EPSP5/EPSP1 ratio was increased by Oxo-M in iSPNs of WT mice ($p = 0.002$, Wilcoxon test; $n = 10$ cells from 4 mice), but not in iSPNs of CDGI-KO mice ($p = 0.25$, $n = 9$ cells from 4 mice) or in iSPNs of WT mice in the presence of VU0255035 ($p = 0.69$, $n = 6$ cells from 3 mice). (K) Box plot showing the effect of Oxo-M on the kinetics of synaptic response. The decay time constant of EPSP5 was significantly increased by Oxo-M in iSPNs of WT mice ($p = 0.002$), but not when CDGI was genetically deleted ($p = 0.65$) or when M1R was pharmacologically blocked ($p = 0.84$). (For interpretation of the references to colour in this figure legend, the reader is referred to the web version of this article.)

An alternative interpretation of these results is that the failure to induce potentiation in iSPNs from CDGI knockout mice was due to saturation of the LTP mechanism. If this were the case, then low frequency stimulation (LFS) of glutamatergic synapses should induce depotentiation (Picconi et al., 2003) in iSPNs from CDGI knockout mice, but not in wildtype iSPNs. However, the responses to LFS were indistinguishable in iSPNs from wildtype and CDGI knockout mice, arguing against this alternative interpretation (Fig. S3A).

To ensure that CDGI deletion did not alter the release of acetylcholine (ACh), we used an optical approach that took advantage of a recently developed genetically encoded fluorescent sensor for ACh—iAChSnFR (Borden et al., 2020). iAChSnFR was virally expressed in the dorsolateral striatum of wildtype and CDGI knockout mice. Three to five weeks later, *ex vivo* parasagittal slices were examined using two-photon laser scanning microscopy and time-series imaging (Fig. 3E). ACh release was evoked with a train of 20 electrical stimuli (1 ms × 50
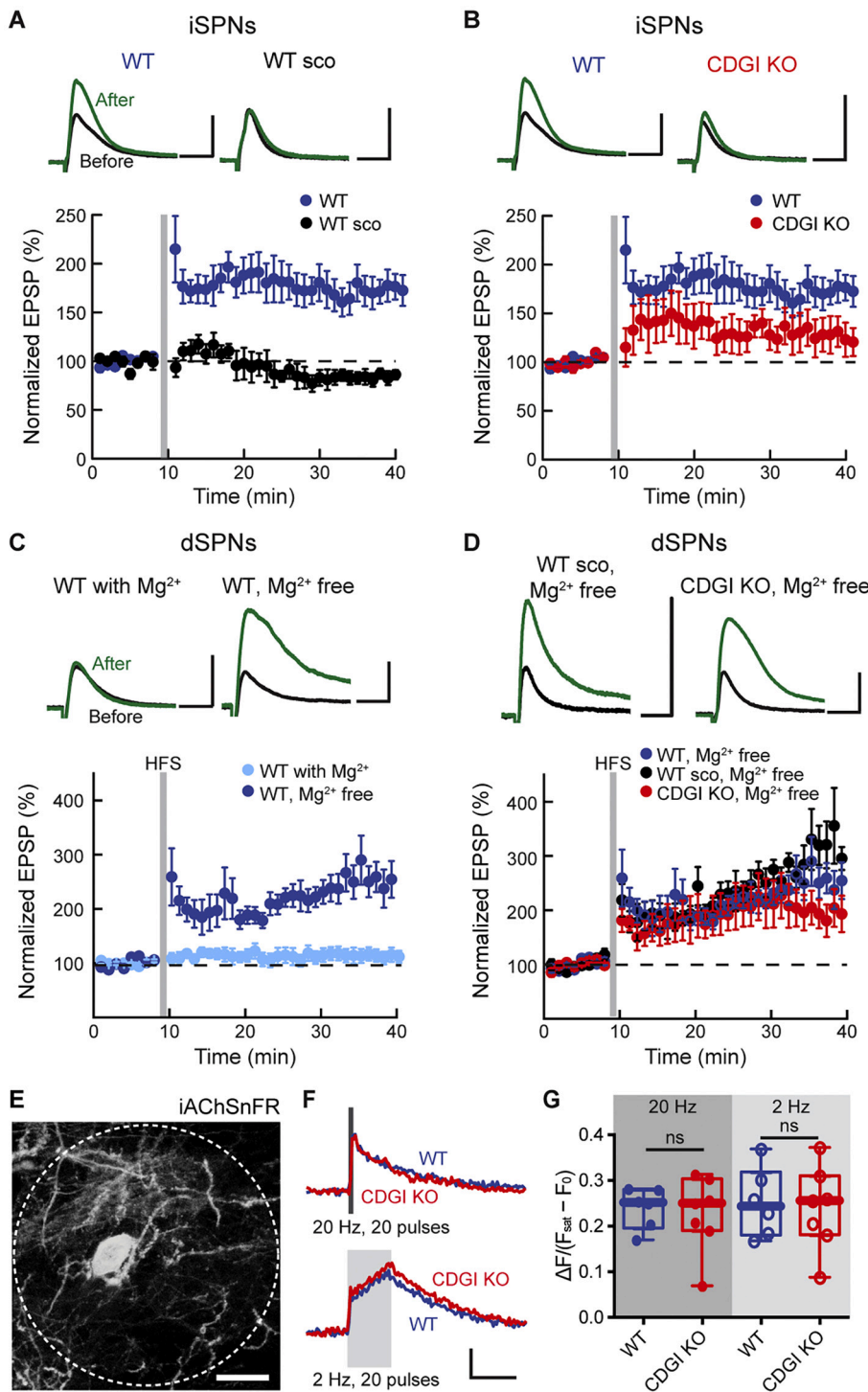
**Fig. 3.** M1R-CDGI signaling is required for full induction of LTP in iSPNs, but not in dSPNs. (A) In normal ACSF (1 mM Mg$^{2+}$), LTP was induced in iSPNs from wildtype (WT) mice ($n = 9$ cells from 7 mice) by HFS (100 Hz for 1 s) paired with current injection (1–2 nA, 1 s), which was repeated four times with 20 s intervals. The LTP induction protocol is indicated by a grey bar. The LTP was blocked by muscarinic antagonist scopolamine (sco, 10 μM, $n = 6$ cells from 4 mice). Data points are mean ± SEM. Samples of averaged EPSP traces before and 30 min after induction are shown at the top. Scale bars, 5 mV × 20 ms. (B) In CDGI knockout (KO) mice ($n = 6$ cells from 4 mice), LTP in iSPNs was impaired. (C) In normal ACSF (1 mM Mg$^{2+}$), LTP could not be induced in dSPNs of WT mice ($n = 7$ cells from 4 mice). In nominal 0 mM Mg$^{2+}$ solution, a robust LTP was induced in dSPNs from WT mice ($n = 6$ cells from 3 mice) by three trains of HFS (100 Hz for 1 s) with 20 s interval (indicated by a grey bar). (D) Genetic deletion of CDGI or scopolamine did not affect LTP in dSPNs (both $n = 6$ cells from 3 mice). (E) Sample image showing expression of ACh sensor iAChSnFR by SPNs. ROI is indicated by the dashed circle. Scale bar = 20 μm. (F) Sample traces of ACh signal (quantified as $\Delta F/(F_{sat} - F_0)$) in response to a train of 20 electrical stimulations (20 Hz and 2 Hz, indicated respectively by dark and light grey bars) in acute slices from WT (blue) and CDGI KO (red) mice. Scale bars, $0.1\Delta F/(F_{sat} - F_0)$ x 10 s. (G) Box plot showing amplitudes of $\Delta F/(F_{sat} - F_0)$ in WT and CDGI KO mice with two stimulation paradigms. ns, not statistically different; Mann-Whitney test. (For interpretation of the references to colour in this figure legend, the reader is referred to the web version of this article.)

μA, at 2 Hz or 20 Hz) delivered through a stimulating electrode placed near (~200 μm) the imaged region. In slices from both wildtype and CDGI knockout mice, the iAChSnFR signal rose rapidly with stimulus onset, decayed when the stimulation ended and returned to baseline within about a minute (Fig. 3F). The iAChSnFR signal was indistinguishable in wildtype and CDGI knockout slices (Figs. 3F,G), strongly suggesting that CDGI had not influenced plasticity indirectly by altering ACh release.

To ensure that other forms of synaptic plasticity were intact, endocannabinoid-mediated long-term synaptic depression (eCb-LTD) was examined in *ex vivo* brain slices using standard approaches

(Calabresi et al., 1992b; Gerdeman et al., 2002). LTD induction was intact in CDGI knockout mice (Fig. S3B).

### 2.5. CDGI deletion altered network control of DA release in the striatum

Given the tie between the muscarinic cholinergic system and both DA and CDGI in the striatum (Gerber et al., 2001; Shin et al., 2015; Zhang et al., 2002), we examined whether CDGI deletion affected DA release in the striatum. We reasoned that the suppression of iSPN excitability induced by CDGI deletion could trigger compensatory network mechanisms aimed at fulfilling the functional role of iSPNs in

movement control. One way in which iSPN excitability could be restored would be by reducing striatal DA release (Klaus et al., 2019; Stoof and Kebabian, 1981). If this line of reasoning were correct, *in vivo* basal DA levels should be reduced, whereas they should be unchanged in *ex vivo* preparations in which DA terminal excitability has been dissociated from the network mechanisms controlling DA release.

To test this hypothesis, striatal DA release was measured in *ex vivo* and in *in vivo* preparations. First, fast-scan cyclic voltammetry in *ex vivo* striatal slice preparations (Figs. 4A-C) was used to measure DA release evoked in response to single stimuli and trains of stimuli designed to emulate phasic firing (4 and 10 pulses of 100 Hz). The release with single and multiple stimuli was not significantly different in striatal sections from CDGI knockout and wildtype control mice (Figs. 4A,B). Moreover, paired pulse depression was not different from controls in CDGI knockouts at inter-pulse intervals ranging from 1 to 60 s (Fig. 4C). Thus, evoked DA release appeared to be normal at our level of detection in the CDGI knockout, suggesting that the dopaminergic terminals did not have intrinsic abnormalities. This finding is consistent with the fact that CDGI expression in mice has not been observed in dopaminergic neurons themselves (Kawasaki et al., 1998). Next, in awake, resting CDGI knockouts and controls, extracellular DA levels in the striatum were assessed using microdialysis. Resting extracellular DA levels in CDGI knockout mice were half those in wildtype mice (Fig. 4D). Total DA content and catechol-*O*-methyl transferase (COMT) activity were similar in CDGI knockouts and controls (Fig. S4). Thus, the CDGI knockouts had reduced levels of extracellular DA in tests in *in vivo* preparations, but not in *ex vivo* preparations, suggesting that striatal dysfunction resulting from the deletion of CDGI triggered network-level changes that lowered DA release in the striatum.

### 2.6. CDGI deletion impaired striatum-based learning

Striatal activity is known to be important in learning and plasticity, and it was thus natural to test different forms of learning. Moreover, striatal M1R signaling has been implicated in the acquisition and reversal of several forms of response learning (Lv et al., 2017; McCool et al., 2008; Tzavos et al., 2004). Given these ties, we turned to three different behavioral tests. First, we adopted the classic cross-maze task developed to discriminate putative habit-based, procedural, egocentric

striatal learning mechanisms from putative allocentric, 'declarative' hippocampal learning mechanisms (Packard and McGaugh, 1996). We trained the constitutive CDGI deletion mutants and sibling controls to learn how to navigate a maze for a food reward using self-referential, egocentric cues (*e.g.*, left-right). Wildtype mice rapidly learned an egocentric T-maze task, but CDGI knockout mice were significantly slower (Fig. 5A). In a reversal learning test and in an allocentric maze task, however, the performance of CDGI knockout and wildtype mice was indistinguishable (Figs. 5B,C). This pattern of results suggests that the CDGI deletion had selective effects and that the temporal dynamics of the maze learning were altered (Schreiweis et al., 2014).

Another type of motor learning that involves the striatum is learning how to link a sequence of motor acts together to form a behavioral repertoire (Barnes et al., 2005; Graybiel, 1998; Graybiel and Grafton, 2015; Martiros et al., 2018). To assess this form of learning, we used a peg-wheel running assay (Kitsukawa et al., 2011; Nakamura et al., 2017). In this task, the arrangement of the wheel's left and right footstep pegs can be changed to test the ability to learn different running patterns (Fig. 5D). Learning was assessed by computing the variance in the timing of paw-placement on the pegs. The CDGI knockout mice did not differ significantly from wildtypes in performance of complex peg-running tasks (Fig. 5E). However, when the whiskers of the mice were clipped before they were tested, forcing mice to rely upon proprioceptive cues (Kincaid and Wilson, 1996; Moussa et al., 2011; Packard and McGaugh, 1996), the CDGI knockout mice again learned the task more slowly (Fig. 5E and Fig. S5). Thus, mice lacking CDGI have a deficit in learning sequential motor behaviors when critical sensory cues were not available.

### 2.7. CDGI deletion enhanced behavioral responses to psychomotor stimulants

Given its rich innervation by dopamine-containing axons, striatal function is profoundly affected by psychomotor stimulants, such as amphetamine and cocaine. Psychomotor stimulants differentially affect immediate-early gene (IEG) expression in striosomes relative to their expression in the matrix, scored as a ratio (Crittenden and Graybiel, 2016; Graybiel, 1998, 2008; Saka et al., 2004). This activation depends in part upon cholinergic interneurons and M1R signaling, as ablation of
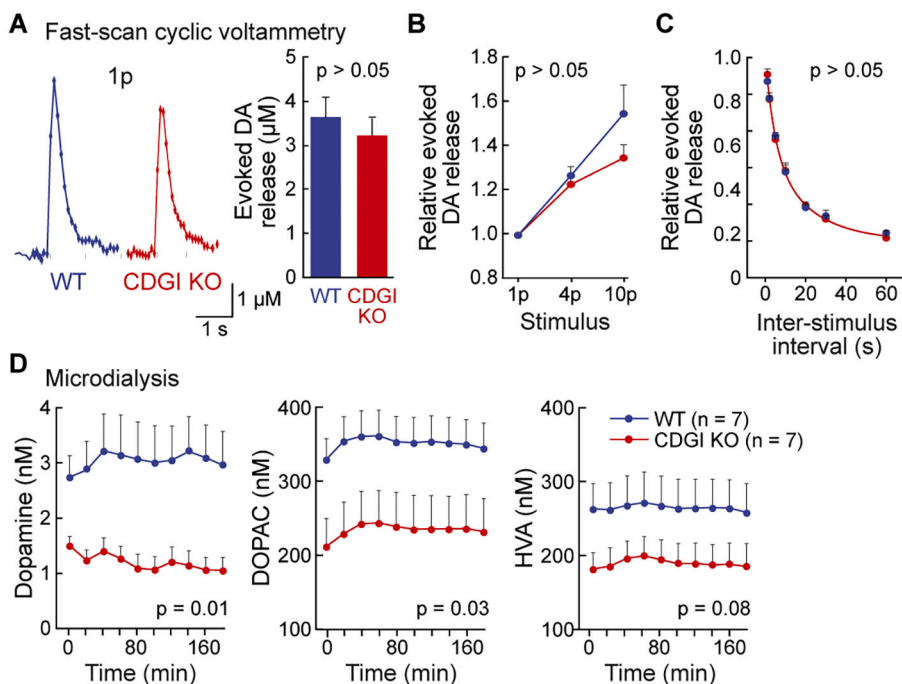


**Fig. 4.** CDGI knockout mice have normal evoked DA release but diminished extracellular DA *in vivo*. (A) Examples (left) and averages (right) of DA release in response to a single pulse (1p) in wildtype (WT, blue) and CDGI knockout (KO, red) mice. (B) DA release in response to a single pulse (1p) or train stimuli (4 or 10 paired stimuli at 100 Hz, 4p and 10p, respectively) was not significantly different between WT and KO mice. $n = 14$ slices for 1p, $n = 8$ slices for 4p and for 10p with slices taken from 5 mice per genotype per experiment. By two-tailed *t*-test, $p = 0.58$ for 1p; $p = 0.57$ for normalized 4p; $p = 0.19$ for normalized 10p. (C) Paired-pulse stimulation showed equivalent depression of evoked DA release between genotypes ($p > 0.05$, Student's two-tailed *t*-test, $n = 7$ slices from each of 5 mice per genotype). (D) *In vivo* microdialysis in the dorsal striatum showed reduced DA and DOPAC and a trend for reduced HVA in KO mice, relative to WT mice. *P* values were calculated by Student's unpaired, two-tailed *t*-tests between average values. Error bars show SEM. (For interpretation of the references to colour in this figure legend, the reader is referred to the web version of this article.)
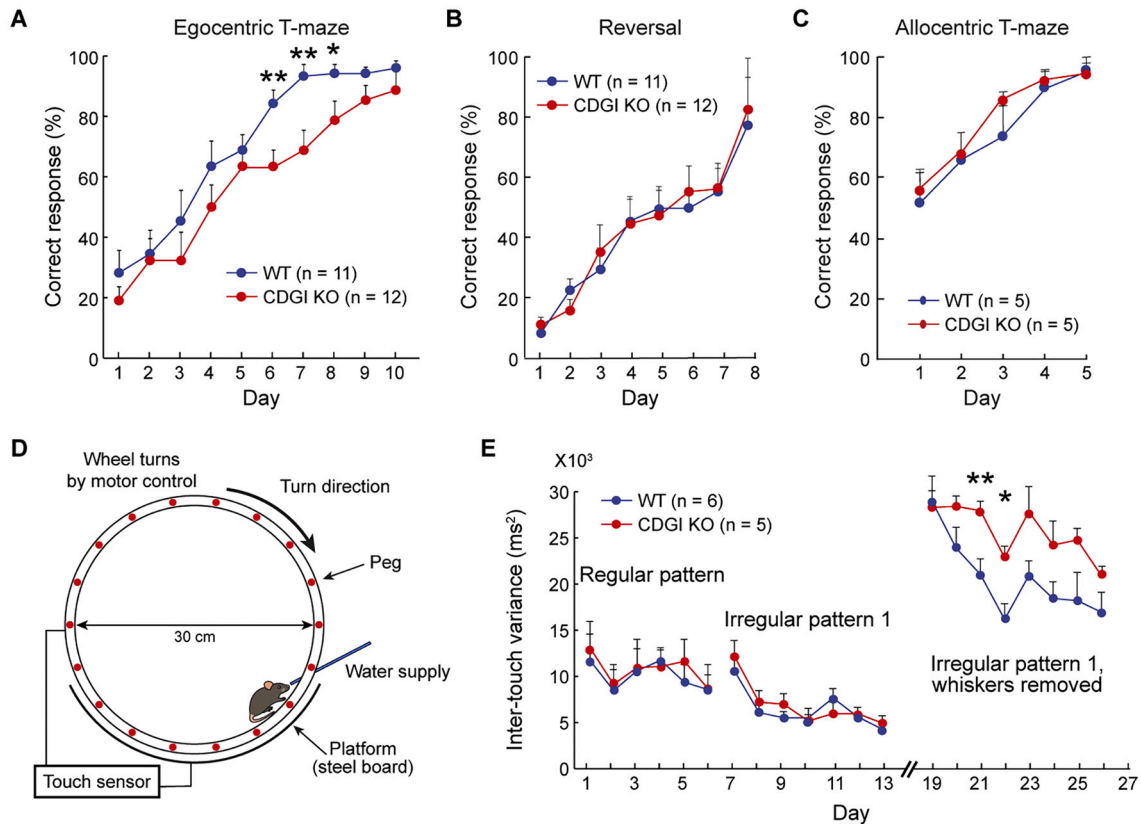
**Fig. 5.** CDGI knockout mice exhibit deficits in striatal learning. (A) In an egocentric T-maze task, CDGI knockout (KO, red) mice learned more slowly than wildtype (WT, blue) mice. $p < 0.05$ by ANOVA; $**p = 0.009$ on day 6; $**p = 0.006$ on day 7; $*p = 0.04$ on day 8 by unpaired, two-tailed Student's t-test. Error bars show SEM. (B) Following the acquisition of the egocentric learning task (A), the rewarded arm was switched to test reversal learning, for which WT and CDGI KO mice showed equivalent acquisition. $p > 0.05$ on all days by unpaired, two-tailed Student's t-test. (C) CDGI KO mice learned to navigate an allocentric, hippocampus-dependent, T-maze at the same rate as sibling controls. Genotype effect: $p = 0.588$, session effect: $p < 0.001$, genotype-by-session interaction effect: $p = 0.713$, ANOVA. (D) Illustration of the motor sequence task on a peg-wheel. (E) Mice were trained in a running wheel with unevenly spaced foot-rungs and learning was measured as a reduction in the variance of paw placement on a designated rung. Intact KO and WT mice learned at equivalent rates; after whisker-cutting, KO mice showed delayed re-acquisition. $**p = 0.01$ and $*p = 0.02$ by unpaired, two-tailed Student's t-test between genotypes. Numbers of mice tested are shown in panel keys. (For interpretation of the references to colour in this figure legend, the reader is referred to the web version of this article.)

cholinergic interneurons or deletion of M1Rs increases the stimulatory effects of amphetamine (Gerber et al., 2001; Xu et al., 2015). Such treatments also disrupt the pattern of IEG expression and the levels of confined, repetitive behavior (stereotypy) induced by DA receptor agonists (Aliane et al., 2011; Saka et al., 2002). We treated wildtypes and CDGI knockouts with high and intermediate doses of amphetamine that are known to induce stereotypy. Mice with global deletion of CDGI manifested increased stereotypic behavior, and decreased distance traveled, as judged both by video analysis (Figs. 6A and S6A,B,D,E) and automated distance-traveled measurements (Figs. 6B and S6C,F,G) relative to wildtype mice.

To determine whether amphetamine-induced stereotypies reflected abnormal brain development arising from the loss of CDGI expression in prenatal and early postnatal mice, we also tested mice from the mouse line with a conditional, postnatal deletion of CDGI. As with mice having a global CDGI knockout, the mice with the conditional CDGI knockout responded to amphetamine treatment (7 mg/kg) with more focal stereotypies (Figs. S6H,I) and less ambulation than their wildtype littermates (Figs. S6J,K). The differential effects of amphetamine on the CDGI knockout mice were not a consequence of alterations in amphetamine pharmacokinetics (Fig. S6L) or DA metabolism (Fig. S4). This impact of CDGI deletion on the response to amphetamine could reflect network effects of CDGI absence; in particular, it is consistent with the requirement for CDGI to have normal LTP in iSPNs, known to mediate movement suppression. M1R cholinergic signaling is also critical for cocaine seeking. The effects of cocaine self-administration are negatively

regulated by striatal cholinergic signaling and M1Rs (Joseph and Thomsen, 2017; Thomsen et al., 2010; Thomsen et al., 2012; Weikop et al., 2020). We used a self-administration protocol (Thomsen et al., 2005) to test for this effect, and asked whether or not M1R signaling would suppress cocaine self-administration in CDGI knockout mice. As expected, when wildtype mice were given the M1R allosteric agonist VU0357017 by systemic injection, they self-administered less cocaine than controls (Figs. 6C,D). In sharp contrast, in the CDGI knockouts, self-administration of cocaine was unaffected by VU0357017 agonist treatment (Figs. 6C,D). When cocaine was replaced with saline in the self-administration procedure, CDGI knockout mice extinguished nose-poking behavior normally (Figs. 6C,D). These findings are consistent with the proposition that CDGI regulation of M1R signaling in iSPNs is critical to the effects of psychomotor stimulants on behavior and drug-seeking.

## 3. Discussion

Our findings demonstrate that CDGI plays a key role in dendritic M1R-mediated modulation of iSPNs and exerts a profound effect on the activity of neurons, circuits and behavior. Three observations led to this conclusion. First, the deletion of CDGI selectively disrupted M1R-evoked dendritic signaling in iSPNs, leaving somatic M1R-evoked signaling intact. This deficit diminished iSPN synaptic integration and prevented full induction of LTP at iSPN glutamatergic synapses. Second, CDGI deletion impaired motor sequence and maze learning by the mice
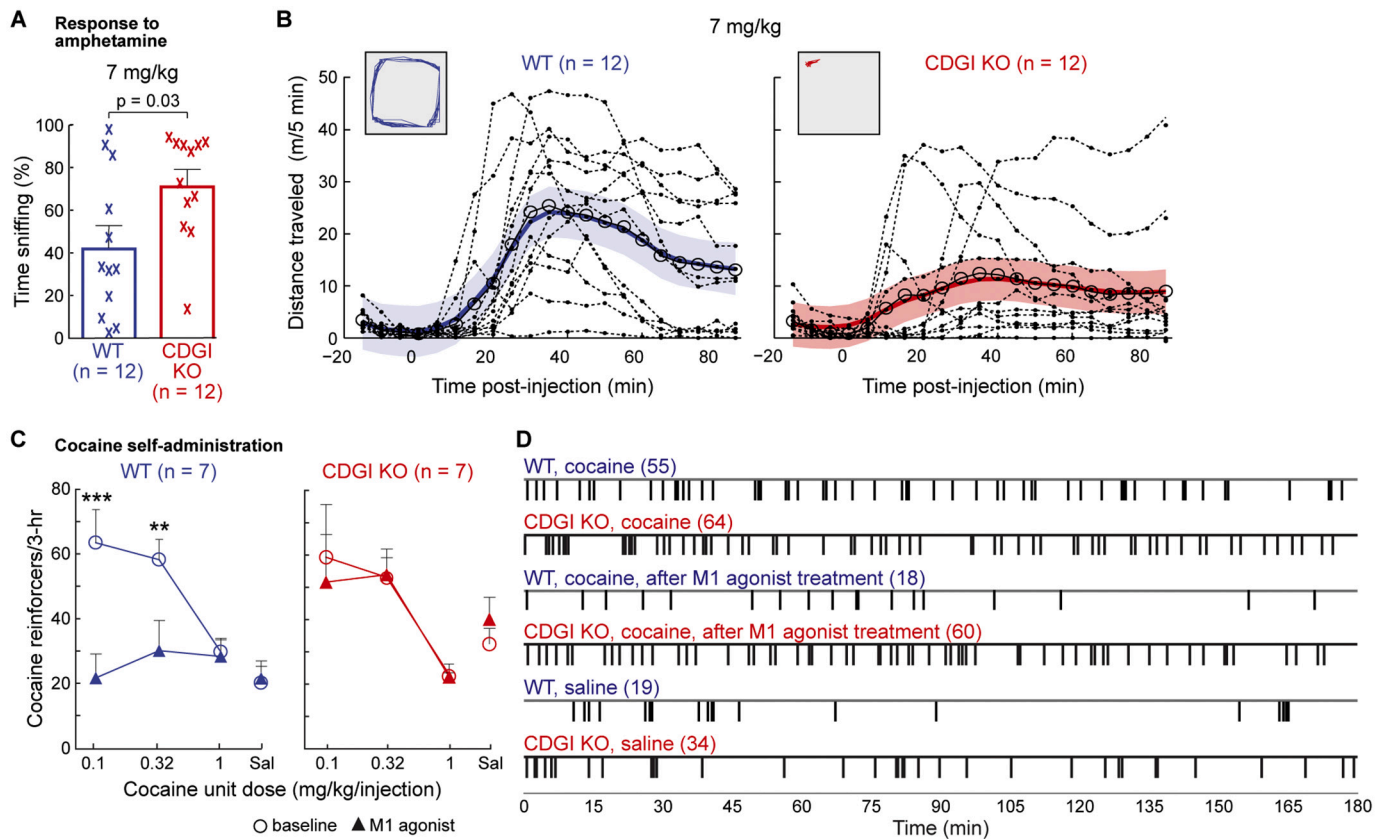
**Fig. 6.** CDGI knockout mice have heightened stereotypy response to amphetamine and fail to suppress cocaine self-administration in response to M1R activation. (A) The proportion of time spent engaging in stereotypic sniffing, scored by videotape observation at 50–52 min post-injection, was higher in CDGI knockout (KO) mice than in wildtype (WT) siblings after acute amphetamine (7 mg/kg). P value was calculated by two-tailed Mann-Whitney $U$ test. Error bars show SEM. (B) In response to high-dose amphetamine (7 mg/kg), KO mice engaged in less locomotion than WT mice, consistent with increased stereotypy. Dotted lines represent raw data from each mouse; large open circles are population means; colored lines are random effects estimates of the median with 90% confidence intervals. Insets show sample open-field tracker plots (50–55 min post-injection). See between group comparisons in Fig. S6C. (C) Both WT and KO mice self-administered cocaine dose-dependently (cocaine dose, $F(3,18) = 6.67$, $p = 0.003$ and $F(3,18) = 6.76$, $p = 0.003$, respectively). The M1-selective agonist VU0357017 suppressed cocaine self-administration in the WT mice only (treatment, $F(1,6) = 9.52$, $p = 0.02$; treatment-cocaine interaction $F(3,18) = 9.29$, $p = 0.0006$). $**p < 0.01$ and $***p < 0.001$ vs. cocaine alone (repeated measures ANOVA and Bonferroni post-hoc test). (D) Examples of sessions from WT and KO mice showing each nose-poke (tick-marks) for self-administration of cocaine (0.32 mg/kg/infusion), cocaine after VU0357017 treatment and saline after extinction of cocaine delivery. The numbers in parenthesis correspond to the total number of reinforcers earned in the session. Numbers of mice tested are shown in panel keys.

without affecting the movements involved in the maze running and without affecting out-of-task motor activities. Third, the CDGI knockout mice exhibited increased stereotypic behaviors following administration of the psychomotor stimulant, amphetamine, and they failed to be rescued from cocaine self-administration by M1R agonist treatment, in sharp contrast to their wildtype controls. These findings demonstrate that CDGI is a potent regulator of cholinergic function in the striatum mediated by indirect pathway-related circuits. The regulatory functions of CDGI, affecting M1R muscarinic actions on iSPNs in the striatum, affect behavioral balance across motor and psychomotor domains, and affect cellular and behavioral features of striatal memory processing. These functions of CDGI, together with its linkage to both HD and LID in parkinsonian states and its relatively confined expression within the striatum and adjacent olfactory structures, point to CDGI as a promising therapeutic target.

### 3.1. CDGI transduction of M1R signaling is consistent with cholinergic-rich features of the matrix compartment

The striatum is placed in a crucial position within the circuitry of the basal ganglia, as it receives massive inputs from the neocortex and thalamus and from aminergic neuromodulators including DA, and it in turn can control the output nuclei of the basal ganglia either directly or

indirectly. Much of this striatal circuitry involves the large extra-striosomal matrix compartment, which is viewed as the principal sensorimotor and associative component of the striatum. The matrix compartment contains most of the cell bodies of the cholinergic interneurons of the striatum and their local processes, and strongly expresses markers of cholinergic transmission, the attribute leading to their discovery in the human striatum (Graybiel and Ragsdale, 1978). M1Rs are robustly expressed by matrix iSPNs (Oldenburg and Ding, 2011), which, like dSPNs, express CDGI (Crittenden et al., 2010; Toki et al., 2001). Proteins associated with cholinergic signaling (e.g., choline acetyltransferase and acetylcholinesterase) are, like CDGI, matrix-enriched (Graybiel et al., 1986; Graybiel and Ragsdale Jr., 1978). Cholinergic innervation is derived largely from local cholinergic interneurons, but includes also cholinergic fibers originating in the midbrain, including from the pedunculopontine nucleus (Dautan et al., 2020; Dautan et al., 2014). Here we demonstrate that CDGI, itself matrix-enriched, is critical to dendritic M1R signaling in iSPNs. We note that the dendrites of the cholinergic interneurons are generally confined to the matrix compartment, but their axons appear in both compartments, consistent with the idea that they could exert cross-compartment effects (Crittenden et al., 2014). Thus, the effects of M1R signaling on CDGI that we have found could be important for this cross-talk as well. We were not able to differentiate striosomal and matrix iSPNs in our

experiments, and we emphasize that with our testing protocols, we could not cover all possible cholinergic effects of CDGI deletion. Nevertheless, our findings demonstrate a critical and multi-faceted requirement for CDGI in the effects of cholinergic function in the striatum aimed at regulation of iSPNs *via* M1Rs.

### 3.2. CDGI mediates dendritic M1R signaling in iSPNs

CDGI activation by $Ca^{2+}$ should be mediated by G-protein coupled receptors (GPCRs) that activate phospholipase C (PLC) isoforms and generate this second messenger (Rhee, 2001). Early work in non-neuronal cells suggested that the effects of M1R signaling, which activates $G_{q/11}$ proteins and PLC, were CDGI-dependent (Guo et al., 2001; Kawasaki et al., 1998). Remarkably, the M1R coupling to CDGI predicted by this earlier work was found in the striatum. Deletion of CDGI selectively disrupted the capacity of iSPN M1Rs to suppress the opening of dendritic Kir2 $K^+$ channels, which control the input impedance of iSPN dendrites (Shen et al., 2020; Shen et al., 2007). Precisely how CDGI deletion disrupted M1R modulation of Kir2 $K^+$ channels remains to be determined. It is known that PLC activation and depletion of membrane $PIP_2$ decreases Kir2 $K^+$ opening (Hansen et al., 2011; Shen et al., 2007). However, CDGI is thought to be downstream of this signaling event and to be a positive modulator of Rap1 signaling, which in turn can regulate Rac1 (Stefanini et al., 2012). Rac1 can down-regulate surface expression of Kir2 $K^+$ channels (Boyer et al., 2009), providing a complementary mechanism to $PIP_2$ depletion by which CDGI could be modulating dendritic excitability. We found that the capacity for M1Rs to decrease the opening of nominally somatic Kv7 $K^+$ channels was unaffected by CDGI deletion, suggesting that this modulation was likely to be solely dependent upon membrane depletion of $PIP_2$ (Hansen et al., 2011). $PIP_2$ has been shown to bind to CDGI in some cell types (Sarker et al., 2020), raising the possibility that depletion of $PIP_2$ in the cell body blocks $Ca^{2+}$-mediated CDGI activation.

Unlike in iSPNs, measurements in dSPNs did not show significant effects from CDGI deletion, despite clear evidence that dSPNs express CDGI (Crittenden et al., 2010; Kawasaki et al., 1998; Toki et al., 2001). In part, this difference is attributable to the subcellular distribution of M1Rs in dSPNs. Although capable of modulating somatic excitability in dSPNs, M1R signaling does not discernibly modulate dSPN dendritic excitability (Day et al., 2008; Shen et al., 2007). The predominant muscarinic receptor in dSPNs is the M4 muscarinic receptor (M4R), which activates $G_{i/o}$ proteins that inhibit dendritic D1 DA receptor signaling and adenylyl cyclase activation (Shen et al., 2015). Additional studies will be required to determine whether CDGI contributes to the intracellular signaling of other $G_{q/11}$-coupled GPCRs known to be expressed by dSPN dendrites, including type 1/5 metabotropic glutamate receptors (mGluR1/5) (Paquet and Smith, 2003).

### 3.3. CDGI is necessary for full induction of LTP in iSPNs

Plasticity at corticostriatal glutamatergic synapses on SPNs is thought to underlie striatum-based learning and memory (Kreitzer and Malenka, 2008; Yin and Knowlton, 2006). As in other regions of the brain, both LTP and LTD can be induced at these glutamatergic synapses. At least two forms of LTD have been described in SPNs (for review, see (Zhai et al., 2018)). The most completely characterized one of these (eCb-LTD) depends upon the activation of mGluR1/5 receptors and the suppression of M1R signaling in iSPNs (Augustin et al., 2018; Gerdeman et al., 2002; Kreitzer and Malenka, 2005; Shen et al., 2008; Wang et al., 2006). Thus, CDGI deletion and disruption of M1R signaling should be permissive for eCb-LTD. In accordance with this prediction, when we examined eCb-LTD in SPNs from CDGI knockout mice by high frequency stimulation of overlying cortex, we found it indistinguishable from that in wildtype mice. M1R-dependent eCb-mediated synaptic plasticity at inhibitory synapses onto SPNs (Narushima et al., 2007) was not examined here. A direct alteration in DA signaling, which also can impact LTD

induction in both iSPNs and dSPNs, was likely not a factor based on our findings of normal DA release in the *ex vivo* brain slices from CDGI knockout mice used to assess plasticity.

Our evidence showed clearly that CDGI deletion disrupted the full induction of corticostriatal LTP in iSPNs. In wildtype iSPNs, pairing high frequency stimulation of cortical inputs with postsynaptic depolarization induced robust LTP in iSPNs. The induction of LTP was dependent upon M1Rs, as antagonizing them with scopolamine blocked induction. This M1R-dependence was not found in dSPNs, in which LTP induction is negatively modulated by dendritic M4Rs (Shen et al., 2015) and unaffected by scopolamine.

The function of M1Rs in iSPN LTP induction is likely to be indirect. By suppressing dendritic Kir2 $K^+$ channels (and possibly other depolarization-activated dendritic $K^+$ channels), M1Rs enhance the summation of the EPSPs evoked by high frequency stimulation and increase the depolarization of iSPN dendrites, allowing relief of the $Mg^{2+}$ block of NMDA receptors, which together are necessary for LTP induction in iSPNs (Calabresi et al., 1992a; Shen et al., 2008; Shen et al., 2020). CDGI deletion disrupted the M1R suppression of dendritic Kir2 $K^+$ channels in iSPNs and, in so doing, likely prevented adequate engagement of NMDA receptors during the induction protocol. It should be noted that the effect of M1R antagonism on LTP was stronger than that of CDGI deletion. This result suggests that either M1R signaling has effects on plasticity that are independent of CDGI (*e.g.*, modulation of somatic excitability) or that deletion leads to compensation. Unlike the LTP induction in iSPNs, LTP induction in dSPNs required nominal removal of extracellular $Mg^{2+}$. The reason for this requirement is not entirely clear, but this result is consistent with previous work (Calabresi et al., 1992a) and the lower intrinsic excitability of dSPNs (Day et al., 2008; Gertler et al., 2008). Established here is a framework for understanding how CDGI shapes striatal plasticity and providing new insight into the asymmetry of the cholinergic modulation of iSPNs and dSPNs (Day et al., 2008; Shen et al., 2015; Shen et al., 2007).

### 3.4. CDGI shapes striatal learning and the response to psychomotor stimulants

CDGI deletion produced clear, nuanced abnormalities in forms of learning classically attributed to the striatum. Deletion of CDGI impaired the ability to learn a simple T-maze task with egocentric cues. CDGI deletion also impaired the ability to learn a complex-sequence stepping task when somatosensory whisking cues were eliminated and the mice were forced to rely only on motor memory or other information. These tests have been shown before to evoke strong and structured repatterning of activity in the striatum of normal mice (Kitsukawa et al., 2011). Striatal cholinergic signaling, particularly that mediated by M1Rs, is itself pivotal for egocentric motor learning and behavioral flexibility with changing reward contingencies (Bradfield et al., 2013; Lv et al., 2017; McCool et al., 2008; Soares et al., 2013; Tzavos et al., 2004). Thus, the behavioral deficits in CDGI deletion mutants are consistent with the importance of CDGI transduction of striatal M1R signaling and synaptic plasticity. CDGI signaling could be involved in other forms of striatal learning and behavioral patterning that depend upon cholinergic signaling, one possibility being adaptibility to change (Bradfield et al., 2013; McCool et al., 2008).

CDGI-mediated modulation of iSPN dendritic excitability is undoubtedly a critical factor in aspects of striatum-dependent learning, but other processes likely are involved as well. One consequence of CDGI-deletion in mice that is likely to be relevant was the network suppression of striatal DA release. Like ACh, DA figures prominently in most forms of striatal synaptic plasticity (Gerfen and Surmeier, 2011). Deficits in DA release diminish the vigor of movement (Panigrahi et al., 2015; Schultz, 2019) and impair the acquisition of egocentric motor tasks (Brasted et al., 1997; Braun et al., 2012). Long-term deficits in DA release combined with normal levels of total DA in the CDGI knockout mice could give rise to compensatory effects such as enhanced

behavioral responses to amphetamine. The mechanisms responsible for the *in vivo* deficit in DA release following CDGI deletion are unclear. One possibility is that the suppression of matrix iSPNs excitability by CDGI deletion results in loss of collateral inhibition of neighboring dSPNs (Taverna et al., 2008) and enhanced inhibition of DA-containing neurons through their projections to the substantia nigra. (Crittenden et al., 2016; Evans et al., 2020; McGregor et al., 2019). Another possibility related to network control is that elevated activity of neurons in the external segment of the globus pallidus, a result of dampened iSPN activation in CDGI knockouts, could lead to elevated inhibition of the nigral dopaminergic neurons and reduced DA release (Evans et al., 2020; Smith and Bolam, 1990; Watabe-Uchida et al., 2012). CDGI deletion in dSPNs also could have important consequences for motor learning that have yet to be discovered.

CDGI deletion clearly increased the idiosyncratic and focused stereotypies evoked by psychomotor stimulant administration. This observation is also consistent with the well-described contribution of cholinergic signaling in regulating stereotypies (Aliane et al., 2011; Crittenden et al., 2014; Janickova et al., 2017; Kuczenski and Segal, 1997, 2001). In addition, CDGI deletion abolished the normal capacity of M1R agonists to reduce cocaine self-administration. These striking effects are consistent with a suppressive effect of iSPNs and the indirect pathway on unwanted movements or actions (Albin et al., 1989; DeLong, 1990; Heinsbroek et al., 2017; Mink, 1996). Thus, our findings point to CDGI as a key regulator of striatal networks engaged by psychomotor stimulants.

CDGI is expressed broadly in the prenatal rodent brain, and modestly in brain regions outside the striatum in the adult, raising the possibility that the phenotypes in global CDGI knockout mice could be owing to loss of CDGI in cell types other than mature SPNs. We confirmed that this is not the case for amphetamine-induced stereotypy. Conditional CDGI^flox/flox^Cre(+) mice in which CDGI expression was lost only after birth, and maintained in the cerebral cortex, showed severe stereotypies relative to CDGI^flox/flox^Cre(−) sibling control mice. Although other tests were performed only in global CDGI knockout mice, the findings are nevertheless directly relevant to humans lacking CDGI expression (Canault et al., 2014; Crittenden et al., 2019).

### 3.5. Translational implications

The identification of CDGI as an effector of M1R signaling in iSPNs has strong implications for work on clinical disorders. Our data from global and post-natal striatal deletion of CDGI are consistent with an M1R-CDGI signaling cascade in the repression of extreme repetitive behaviors and self-administration induced by psychomotor stimulants. Intensive research to develop small molecules that target specific muscarinic receptor subtypes such as M1R is motivated by preclinical results from rodent models of psychiatric disorders including drug addiction (Choy et al., 2016; Moran et al., 2019; Stoll et al., 2018). However, side-effects from peripheral M1R targeting have proven to be a major stumbling block in the advancement of this approach (Moran et al., 2019). Therapeutic targeting of CDGI could potentially alleviate this problem by providing a tissue-specific entrée to the M1R signaling cascade.

The hyperkinetic features of early manifest HD have long been attributed to the preferential dysfunction of iSPNs responsible for suppression of unwanted movement (Albin et al., 1989; Plotkin and Surmeier, 2015; Shen et al., 2015). In mouse models of HD, the dendritic excitability of iSPNs is depressed, and LTP at corticostriatal synapses is impaired (Carrillo-Reid et al., 2019; Plotkin et al., 2014), mimicking the impact of CDGI deletion. CDGI expression is severely down-regulated in HD patients, potentially a compensatory effect (Crittenden et al., 2010; Desplats et al., 2006; Kuhn et al., 2007; Luthi-Carter et al., 2002). But it is not yet clear whether this down-regulation is a cause or consequence of striatal pathophysiology. Striatal cholinergic interneurons are not lost in HD, but proteins associated with ACh release are down-regulated

(Pisani et al., 2007). Moreover, basal ACh release is diminished in HD models (Farrar et al., 2011). Thus, it is possible that the down-regulation of CDGI in HD is a consequence of diminished cholinergic signaling. However, it is also possible that cell autonomous down-regulation of CDGI contributes not only to diminished iSPN excitability, but also to the suppression of cholinergic synaptic markers. To sort out these possibilities, cell-type-specific expression of zinc finger proteins targeting mutant huntingtin (Carrillo-Reid et al., 2019; Zeitler et al., 2019) could be used to dissect cell autonomous and non-autonomous drivers of the CDGI down-regulation.

Another neurodegenerative disorder associated with CDGI dysregulation and altered striatal cholinergic signaling is Parkinson's disease. The hypokinetic features of Parkinson's disease are generally attributed to elevated iSPNs excitability following the loss of striatal DA release, the reverse of the hypoactivity of iSPNs in HD. There are two well-described drivers of this shift: loss of inhibitory D2 DA receptor signaling and enhancement of excitatory M1R signaling (Pisani et al., 2007). Muscarinic receptor antagonists are effective in alleviating motor symptoms of Parkinson's disease, but are not well tolerated because of side-effects (Katzenschlager et al., 2003). CDGI could provide an important alternative target for down-regulating striatal M1R signaling: unlike M1Rs, neuronal CDGI is largely restricted to the striatum and adjoining olfactory structures (Kawasaki et al., 1998), minimizing any off-target effects of down-regulating its function in the brain.

In late-stage Parkinson's patients, LIDs diminish the quality of life, and there are only marginally effective treatments for these complications (Fabbrini et al., 2007). CDGI down-regulation in rodent models of LID is positively correlated with the severity of the abnormal movements (Crittenden et al., 2009). Again, it is unclear at this point whether this change is compensatory or contributory to the network pathophysiology underlying LID. But given that boosting iSPN excitability during the on-state diminishes LID (Alcacer et al., 2017), it is possible that the down-regulation of CDGI (and iSPN excitability) is a cause of the hyperkinetic features of LID. It is notable that a striosome-enriched paralog of CDGI, CalDAG-GEFII (aka RasGRP), is strongly up-regulated in LID models; moreover, the extent of this up-regulation is correlated with the severity of LID (Crittenden et al., 2009). This pattern of dysregulation is consistent with the hypothesis that an imbalance in the activity of matrix and striosomal SPNs contributes to the excessive movement patterns in LIDs (Graybiel et al., 2000).

Our findings collectively suggest that CDGI is a major signaling molecule modulating striatal excitability and plasticity that underlies motor learning and responses to abused psychomotor stimulants. These key functions of CDGI are, we show, to a significant extent attributable to its mediation of cholinergic M1R signaling in iSPNs. Down-regulation of CDGI in iSPNs, which help suppress unwanted movement, can contribute to the hyperkinetic features of early HD and LID. We emphasize that in contrast to widely distributed M1Rs, the narrow forebrain distribution of CDGI, with its strong enhancement in the striatum, makes CDGI an attractive therapeutic candidate target for boosting iSPN excitability in HD and LID. The work presented here creates a platform for exploring this possibility through understanding how CDGI shapes the activity of striatal neurons that profoundly affect action, learning and decision-making in health and disease.

## 4. Materials and methods

### 4.1. Mouse maintenance

All experiments were approved by, and performed in strict accordance with, the Massachusetts Institute of Technology (MIT) Committee on Animal Care, which is accredited by AAALAC International. Mice were group-housed and maintained under a standard light/dark cycle with free access to food and water except during food-reinforced learning and memory experiments, in which cases mice were single-housed. For the cocaine self-administration assay and the total

biogenic amine and amino acid data, CDGI knockout and sibling control mice were in a congenic C57BL/6 J genetic background. For the amphetamine-response experiments, the global CDGI knockouts and sibling controls were in a congenic 129S4 genetic background. Conditional CDGI$^{flox/flox}$Cre(+) knockout mice and CDGI$^{flox/flox}$Cre(−) sibling controls were generated from D1-YAC Cre(+) mice in a C57BL/6 background (gift of Thomas Lemberger) and CDGI$^{flox/flox}$ mice in a 129S4 background. For the slice physiology experiments with identified dSPNs or iSPNs, the CDGI knockout mice in a C57BL/6 J background were crossed to Drd1-tdTomato or Drd2-EGFP BAC transgenic mice (Gong et al., 2003) in a C57BL/6 background. For all other experiments, mice were in an isogenic 129S4 genetic background. Male mice were used for all behavioral and slice physiology experiments, which were initiated prior to the National Institutes of Health policy for the inclusion of both sexes.

### 4.2. Generation of CDGI knockout mice

The CDGI targeting construct was based on a 6.2 kb *Sac*I restriction fragment from the 129Sv/cJ7 mouse chromosome 19 BAC clone 7D23 (Guru et al., 1999) that was subcloned into Bluescript II KS+ plasmid (Stratagene Inc). One loxP site was ligated to a *Hin*dIII site in intron 4 and a loxP-flanked fusion gene for hygromycin resistance, and thymidine kinase was ligated to an *Afl*II site in intron 2. The targeting construct was electroporated into J1 mouse embryonic stem (ES) cells (gift of Prof. Rudolf Jaenisch) that were subsequently grown in hygromycin to select for integration. Resistant ES cell clones were screened for homologous integration by polymerase chain reaction (PCR) and Southern blotting. Clonal populations were transiently transfected with the Cre recombinase vector Pog231, and gancylcovir was applied to select for loss of thymidine kinase. PCR was used to identify deletion clones, two of which were injected into blastocysts by the MIT Department of Comparative Medicine facility. Resulting chimeric mice were crossed to C57BL/6 to test for germline transmission by coat colour, and transmitting males were crossed to 129S4 mice to establish the mutation in a background isogenic with the J1 ES cells. Phenotypic analyses were always performed on sibling progeny from pure 129S4 heterozygous mutant intercross matings. Constitutive CDGI knockout mice were genotyped by PCR with the following three oligonucleotide primers: 5′–aacagttcccaggctagagatagagagttcctcc–3′, 5′–acca gactctaggccagaacctacc–3′, and 5′–agtgtgctgtggtgaaatgcagccattcc–3′. Wildtype mice yielded a 208 base pair product with the first two primers, whereas the knockout yielded a 286 base pair product with the second two primers. Conditional CDGI floxed mice were genotyped by PCR with the two primers 5′–tctcagctagtccatttcccaactagcgagttgc–3′ and 5′–aacagttcccaggctagagatagagagttcctcc–3′ to yield a 650 bp product from the floxed allele and a 594 bp product from the wildtype allele.

### 4.3. Reverse transcriptase polymerase chain reaction

Mouse brain RNA was prepared using the RNAeasy kit (Qiagen). Reverse-transcriptase quantitative polymerase chain reaction (RT-PCR) was performed using the ThermoScript RT-PCR kit (Invitrogen) with two primers flanking the sites where loxP was inserted: 5′–taatacgact cactatagggaggctgagctggttcaagtg–3′ and 5′–atttaggtgacactatagaactgccg cttccacttgtagg–3′.

### 4.4. Western blotting

For harvesting mouse striatal and cortical tissue, mice were deeply anesthetized with pentobarbital (150 mg/kg by intraperitoneal injection), and tissue was dissected on a cold plate prior to freezing in liquid nitrogen and storage at −80 °C. Frozen samples from mice were homogenized in ice-cold modified RIPA buffer (50 mM Tris pH 8.0, 150 mM NaCl, 1% Triton X-100, 0.1% sodium dodecyl sulfate, 1% NaDeoxycholate) with complete protease inhibitor cocktail (Roche) and

centrifuged at 16,000 X g for 10 min to pellet insoluble material. Protein concentration of supernatants was determined by bicinchoninic acid assays (Thermo Fisher Scientific). Proteins were resolved by SDS-PAGE and transferred to PVDF membrane (Millipore) by electroblotting. Blots were incubated overnight, at 4 °C, with antibodies diluted in TBST [10 mM Tris-HCl (pH 8.0), 150 mM NaCl, 0.05% Tween 20)] and 5% bovine serum albumin. Blots were subsequently washed in TBST and incubated with horseradish peroxidase-coupled secondary antibodies (Vector Laboratories, Burlingame, CA) prior to immunodetection with Western Lightening (PerkinElmer Inc.) according to the manufacturer's instructions. Blots were subsequently incubated with anti-β-tubulin (Cell Signaling Technology) to control for protein loading. Antibodies were obtained from the following companies: total GluR1 receptor (Calbiochem), total ERK1/2, phospho-ERK1/2, total JNK, phospho-JNK, total P38, phospho P38, total DARPP-32 and phospho-DARPP-32 (Cell Signaling Technology); GluR2 receptor, phosphor-Ser831 GluR1 receptor, mGluR1 receptor, mGluR5 receptor, M1-type muscarinic receptor, D1-type and D2-type DA receptor (Chemicon); phosphor-Ser845 GluR1 receptor (Novus Biologicals); Rap1, Rap2, CalDAG-GEFII/RasGRP2 (Santa Cruz Biotechnology); phosphor-CREB (Rockland Immunochemicals); and PSD95 (Upstate Biotechnologies).

### 4.5. Immunolabeling

Mouse brain sections were prepared for immunolabeling as previously described (Crittenden et al., 2021; Niemz et al., 2017). The sections were incubated with rabbit polyclonal CDGI antiserum (Crittenden et al., 2004) for approximately 12 h at 4 °C and processed either for immunohistochemistry with ABC amplification (Vector Laboratories) and DAB detection with nickel enhancement or, in conjunction with mouse anti-CalDAG-GEFII antiserum (SC-8430, Santa Cruz Biotechnology), for immunofluorescence with secondary antibodies coupled to ALEXA 564 and ALEXA 488 (Invitrogen). Fluorescent labeling of neurons expressing D1 and D2 DA receptors was detected with mCherry or EGFP filter set in sections from Drd1a-tdTomato and Drd2-EGFP BAC transgenic mice (Gong et al., 2003). Sections were mounted and coverslipped with Eukitt (Electron Microscopy Sciences) following immunohistochemistry, or with Vectashield mounting medium (Vector Laboratories) for confocal detection of genetic fluorescent labeling. The sections were viewed with Olympus BX61 and SZX7 microscopes fitted with an Olympus DP70 camera.

### 4.6. Exon microarray

Striatal tissue was collected in parallel in three different experiments from age-matched male CDGI knockout mice and sibling controls. After dissection, samples were frozen on dry ice and then homogenized in Trizol (Sigma-Aldrich), and total RNA was prepared according to manufacturer's instructions and previously described methods (Cantuti-Castelvetri et al., 2005). Equivalent amounts of RNA from each sample were pooled according to genotype ($n = 4$ of each genotype pooled for two experiments and $n = 3$ of each genotype pooled for one experiment) and given to the MIT BioMicro center to prepare cDNA for hybridization to the Affymetrix GeneChip® Mouse Exon 1.0 ST. The MIT Bioinformatics core facility used Affymetrix Expression Console software to summarize and normalize data from the chips.

### 4.7. Measurements of total and extracellular striatal DA, DOPAC and HVA

For microdialysis, guide cannulae were implanted in the striatum using stereotaxic surgery. After at least one week for post-surgical recovery, the microdialysis probe (CMA/7 probe 1 mm, CMA Microdialysis, Sweden) was lowered into the guide cannula, and microdialysates were collected on ice in perchloric acid (0.5 M) at 20-min intervals at a rate of 1.5 μl/min. Samples collected for the first

hour were discarded, and subsequently collected samples were immediately frozen and kept at −80 °C until high performance liquid chromatography (HPLC) analysis.

For measurements of DA, 3,4-dihydroxyphenylacetic acid (DOPAC) and homovanillic acid (HVA) to assess COMT activity, mice were decapitated 50 min after saline or amphetamine injection, and the striata were dissected on ice and kept at −80 °C until shipment to the laboratory of Prof. Tim Maher (Massachusetts College of Pharmacy and Health Sciences) for HPLC.

For HPLC analysis, microdialysates were injected unmodified, and striatal tissues were homogenized in 0.2 M perchloric acid, 0.2 mM disodium EDTA and 0.2 mM ascorbic acid. Samples were assayed for DOPAC, DA and HVA by HPLC with the potential set at +300 mV with respect to a palladium-hydrogen reference electrode.

### 4.8. Measurements of striatal amino acids and biogenic amines

For measurements of total amino acids and biogenic amines, male mice between 4 and 5 months of age ($n = 11$ wildtypes and 7 knockouts) were sacrificed by cervical dislocation, and striatal tissue was dissected and frozen on dry ice for shipment to the Vanderbilt Neurochemistry core for HPLC measurements.

### 4.9. DA receptor autoradiography

D1- and D2-type DA receptor autoradiography was performed as described in Unterwald et al. (Unterwald et al., 1994; Unterwald et al., 2001). D3 receptor autoradiography was carried out according to the method described by Guitart-Masip et al. (Guitart-Masip et al., 2006). Mouse brains were stored at −80 °C prior to dissection. Mouse brains were mounted on cryostat chucks using embedding matrix, cut on a Reichert and Jung 2800 Frigocut N into 16 μm coronal sections based on the Paxinos and Franklin mouse brain atlas (Paxinos and Franklin, 2001), thaw-mounted onto Fisher superfrost glass slides, air-dried on ice and stored desiccated at −30 °C until assayed. Slide-mounted sections were preincubated in buffer containing 50 mM Tris HCl, 120 mM NaCl, 5 mM KCl, 2 mM CaCl$_2$ and 1 mM MgCl$_2$, pH 7.4, at room temperature for 30 min. Following preincubation, sections were incubated for 45 min at room temperature in the same Tris-salt buffer in the presence of 1 μM mianserin and 5 nM ^{3}H-SCH23390, without and with 10 μM fluphenazine to measure, respectively, total and nonspecific binding for the D1-type DA receptor. For D2-type receptor autoradiography, slides were incubated in the preincubation buffer with 0.001% ascorbic acid, 1 μM mianserin and 5 nM ^{3}H-raclopride without and with 10 μM (+)buta-clamol to measure total and nonspecific binding, respectively. For D3 receptor binding, slides were incubated in the preincubation buffer in the presence of 0.001% ascorbic acid, 5 nM ^{3}H-PD128907 without and with 1 μM (+)butaclamol to measure total and nonspecific binding, respectively. After incubation, slides were washed twice in the Tris-salt buffer on ice for 5 min/wash followed by rinse in ice-cold distilled water. Sections were dried under a cold air stream and allowed to sit overnight at room temperature. Slides for DA receptor autoradiography and tritium standards (Amersham) were exposed to tritium-sensitive film for 7 weeks (D1 receptor), 13 weeks (D2 receptor) or 23 weeks (D3 receptor). Receptor densities were determined by measuring the optical densities of brain regions of interest and by comparing them to the standard curve generated by the tritium standards exposed to the same sheet of film (MCID System, Imaging Research Inc., Cambridge, UK). Differences in mean receptor density values between genotypes were analyzed by an unpaired two-tailed Students *t*-test.

### 4.10. Measurements of serum amphetamine

For serum amphetamine measurements, blood was collected into serum separation tubes (Starstedt AG & Co.) by retro-orbital bleeds from mice under isofluorane anesthesia, 50 min after amphetamine injection.

Amphetamine measurements were performed at NMS Labs (Willow Grove, PA) using liquid chromatography followed by mass spectrometry (LC/MS/MS). Serum aliquots of 50 or 100 μl were diluted to 200 μl with human serum. The dilution was taken into consideration to calculate the final concentrations. An internal standard (D5-Amphetamine) and 10% trichloroacetic acid were added to each sample while mixing vigorously. Samples were centrifuged, and 200 μl of supernatant from each sample was transferred to autosampler vials for analysis. Samples were analyzed using a Waters Quattro Premier tandem mass spectrometer instrument with electrospray ionization, and a Waters Acquity Ultra Performance LC with an Acquity UPLC HSS T3.1, $2.1 \times 50$ mm, and 1.8-μm analytical column. Two ion transitions were monitored for amphetamine and the internal standards to assure that there were no interferences. Each analytical run was independently calibrated at concentrations of 5.0, 10, 20, 50, 200, 500 and 1000 ng amphetamine/ml. Controls were run at 30, 375 and 750 ng/ml. During method validation, this LC/MS/MS method had between-run percent CV's of 6.03, 3.02 and 4.72% at 5.0, 30 and 750 ng/ml, respectively. Amphetamine eluted at approximately 3.5 min and the internal standard co-eluted.

### 4.11. Open-field behavior, rotarod balance and fear conditioning

Horizontal and vertical locomotor activity (distance traveled, rearing) for the evaluation of open-field activity and fear-conditioning tasks was collected *via* the TruScan System (activity boxes surrounded by 2 rings fitted with infrared sensors, Coulbourn Instrument, Allentown, USA). The same system was used to measure 'time spent in the margin' (thigmotaxis) and 'number of center entries' for the assessment of anxiety-related behaviors. For fear-conditioning procedures, mice received 5 tones paired with foot shocks (1 per min) in box A after 2 min of free exploration (baseline A) on day 1. On the morning of the following day, mice were placed in the same box without tone or foot shock for 3 min. In the afternoon of the same day, mice were placed in box B (contextually different), and the tone alone was delivered for 3 min after 2 min free exploration of the new box (baseline B). Percent decrease in distance traveled *versus* baseline in either box was calculated as a measure of association of foot shocks with context or foot shocks with cue. To evaluate motor coordination, mice were placed individually onto an elevated rod accelerating from 4 to 40 rpm over 10 min (Columbus Instruments), and latency to fall was measured.

### 4.12. Home cage scan

Male wildtype and knockout brothers, 6–7 months of age were single-housed for >7 days prior to videoscanning. Lights were out from 7 pm to 7 am, and videotaping occurred from 6 pm to 6 am. Data were analyzed by user-trained CleverSys software as described previously (Steele et al., 2007).

### 4.13. Social interaction and memory test

According to the method described previously (Crawley, 2000), single-housed male mice were placed individually into a large cage with bedding and two small metal wire enclosures inside, and were allowed to acclimate for 20 min. The male was then removed, and an ovariectomized female was placed into the small wire cage prior to returning the male. The male was videotaped for 2 min prior to removal of the female mouse. After 20 min, the same female was re-introduced for 2 min, and this procedure was repeated four times in total prior to introducing a novel ovariectomized female. Videotapes were scored, and the amount of time that the male had nose-contact with the cage containing the female was plotted.

### 4.14. Olfactory acuity test

Wildtype and brother knockout male mice were co-housed and food-

restricted by being given access to food for only one hour per day, plus sucrose pellets sprinkled in their home cage (BioServ). Mice were trained for two days by placing them individually into a clean cage in the morning and, in the afternoon, were given 15 sucrose pellets on top and beneath the bedding. On the following test day, each mouse went through five trials in which it was removed from the cage, a single pellet was buried, and measurements were taken of the time for the mouse to find the pellet after reintroduction to the cage.

### 4.15. Marble burying

Based on a method described previously (Thomas et al., 2009), male mice were placed into a clean cage and given 30 min to habituate. The mouse was removed, and 9 clean marbles were placed, evenly-spaced, on top of the bedding. The mouse was returned to the cage and videotaped for 15 min. The number of marbles visible at the end was reported as an average across trials. Mice were given three trials across three days.

### 4.16. Egocentric and allocentric T-maze tasks

Training was done by an experimenter blinded to genotype, and mice were in mixed-genotype groups. Egocentric T-maze training was conducted in an acrylic cross-shaped maze with white floor and transparent walls. Different departure arms were used so that mice learned to associate the rewarded arm with egocentric cues rather than distal cues. Male mice, food-restricted to reach 85% of their free-feeding weight, were given 3–5 habituation sessions in which they were allowed to move freely in the two T-maze configurations and to consume chocolate milk placed at the end of the goal arms. Mice were rewarded with chocolate milk for turning in a consistent direction (left vs. right), regardless of their start site and the spatial cues. The rewarded direction was randomly assigned at the beginning of the training unless the mouse had developed a turning bias during the habituation, in which case the opposite direction was baited with food-reward for the training. Each mouse received 10 trials (5 trials from each of 2 start sites), with an inter-trial interval of 30–120 s, during each daily session for 10 days.

Allocentric T-maze training was conducted in a water maze filled with white dyed water (21 °C) into which a mouse was placed at the base of the T to begin the trial. The trial was ended when the mouse touched both forepaws to the submerged escape platform (correct choice) or reached the extremity of the other branch of the T (incorrect choice). The platform was located at a constant position in the experimental room, and extra-maze visual cues were provided to instruct the mice of the platform location. Start arms were varied to avert the use of egocentric cues. Percent correct choices and latency to reach one extremity of the T (data not shown) were recorded. Each mouse received 10 trials per day.

### 4.17. Step-wheel training

All procedures were approved and in accordance with guidelines for the conduct of animal research of Osaka University. The investigator training the mice was blinded to their genotypes. As previously described (Kitsukawa et al., 2011), mice were water-restricted and habituated to run on a step-wheel with moveable pegs in order to reach a water spout. Contact of the paw on the last (12th) rung was detected by a voltage change. Mice were trained for 6 days with a regularly spaced rung-pattern followed by 7 days of training with irregularly spaced rung pattern 1, followed by 3 days of training with irregularly spaced rung pattern 2. The whiskers of all mice were then cut off, and the mice were given 2 days in their home cage followed by re-testing for 8 days with irregularly spaced rung pattern 1. The variance of paw-touch to the 12th rung across training was calculated (Nakamura et al., 2017).

### 4.18. Amphetamine treatments

Different groups of male mice (6–10 months old) were used for each drug treatment. All experiments were conducted genotype-blind. Mice were habituated to injection for 3–5 days and placed in TruScan activity monitors for at least 20 min prior to drug injection. D-amphetamine (Sigma-Aldrich) was dissolved in saline and administered at 10 ml/kg body weight intraperitoneally. Distance traveled was computed by infrared photobeam breaks, sampled every 0.5 s. Stereotypies were measured from 2 min videotapes made at 50 min post-injection (peak-stereotypy response period) and rated with a keypad scoring system by a rater blinded to genotype as previously described (Crittenden et al., 2014). Distance-traveled data were analyzed by a state-space model (Kitagawa and Gersch, 1996; Smith et al., 2004). Activity monitor data for distance-traveled were chosen for 21 time-points ($-15$ to 85 min in steps of 5 min) for all wildtype and CDGI knockout mice described in detail (with computer code for this application) previously (Crittenden et al., 2019). Briefly, the model provided a population estimate for the distance-traveled across 21 time-points ($-15$ to 85 min in steps of 5 min) for the wildtype and CDGI knockout groups. Group population estimates were compared using Monte Carlo techniques with between group differences highlighted where $p < 0.05$.

### 4.19. Cocaine intravenous self-administration

All procedures were approved by the McLean Hospital Institutional Animal Care and Use Committee. Mice were trained and tested as previously described under an FR 1 schedule of reinforcement in daily 3 h sessions, 5–6 days/week (Thomsen et al., 2010). VU0357017 was synthesized at Vanderbilt University (Lebois et al., 2010), dissolved in sterile water (made fresh daily) and administered subcutaneously at 5.6 mg/kg, 15 min before the test session.

### 4.20. Fast-scan cyclic voltammetry

All voltammetric experiments were approved and performed in strict accordance with the Institute of Comparative Medicine Laboratory Animal Resources at Columbia University.

Striatal DA release was studied in two to five month old male knockout and wildtype mice. Recordings were obtained from the striatum in the first three most rostral coronal slices (300 μm). Three sites in the dorsal striatal region of each slice were measured and averaged. Slices were allowed to recover for 1.5 h in a holding chamber in oxygenated artificial cerebrospinal fluid (ACSF) at room temperature, and then were placed in a recording chamber and superfused (1 ml/min) with ACSF (in mM: NaCl 125, KCl 2.5, NaHCO$_3$ 26, CaCl$_2$ 2.4, MgSO$_4$ 1.3, KH$_2$PO$_4$ 0.3, glucose 10) at 36 °C.

As described previously (Zhang and Sulzer, 2003), disk carbon fiber electrodes of 5 μm diameter with a freshly cut surface were placed into the dorsal striatum about 50 μm into the slice. For cyclic voltammetry, a triangular voltage wave ($-400$ to $+900$ mV at 280 V/s versus Ag/AgCl) was applied to the electrode every 100 ms. Current was recorded with an Axopatch 200B amplifier (Axon Instrument, San Jose, CA), with a low-pass Bessel Filter setting at 10 kHz, digitized at 25 kHz (ITC-18 board, InstruTech Corporation). Triangular wave generation and data acquisition were controlled by a computer running a house-written IGOR program (WaveMetrics). Striatal slices were electrically stimulated every 2 min with either a single pulse stimulation or a paired stimulus by an Iso-Flex stimulus isolator triggered by a Master-8 pulse generator (A. M.P.I.) using a bipolar stimulating electrode placed ~100 μm from the recording electrode. Background-subtracted cyclic voltammograms served to identify the released substance. The DA oxidation current was converted to concentration based upon a calibration of 5 μM DA in ACSF after the experiment.

### 4.21. Corticostriatal LTD induction

Experiments were approved and performed in strict accordance with the procedures put forward by the Italian Health Ministry. Corticostriatal EPSPs were evoked by a stimulating electrode placed in cortical regions close to the recording electrode. Bicuculline (10 μM) was added to ~50% of the experiments to test for contamination of the EPSPs by GABA$_A$ receptor-mediated depolarization. The addition of bicuculline did not have an effect on EPSPs, thus data obtained with and without the drug were pooled. For HFS, 3 stimulus trains were applied (3 s duration, 100 Hz frequency, 20 s intervals). HFS protocol was delivered in the presence of 1.2 mM external magnesium to optimize the appearance of LTD.

### 4.22. Slice electrophysiology in identified D1 and D2 SPNs

Animal use procedures were reviewed and approved by the Northwestern Institutional Animal Care and Use Committee. CDGI knockout mice expressing one copy of tdTomato or EGFP under control of Drd1a or Drd2 receptor regulator elements were used for cell type-specific physiological studies at 8–12 weeks of age. Mice were deeply anesthetized with a mixture of ketamine (100 mg/kg) and xylazine (7 mg/kg) and perfused transcardially with ice-cold sucrose-based cutting solution containing (in mM): 181 sucrose, 25 NaHCO$_3$, 1.25 NaH$_2$PO$_4$, 2.5 KCl, 0.5 CaCl$_2$, 7 MgCl$_2$, 11.6 sodium ascorbate, 3.1 sodium pyruvate and 5 glucose (305 mOsm/l). Parasagittal slices (280-μm thick) were sectioned using a vibrotome (Leica VT1200). After cutting, slices were incubated at 34 °C for 40 min in ACSF containing (in mM): 124 NaCl, 3 KCl, 1 NaH$_2$PO$_4$, 2.0 CaCl$_2$, 1.0 MgCl$_2$, 26 NaHCO$_3$ and 13.89 glucose, after which they were stored at room temperature until recording. External solutions were oxygenated with carbogen (95%CO$_2$/5%O$_2$) at all time.

Individual slices were transferred to a recording chamber and continuously superfused with ACSF (2–3 ml/min, 30–32 °C). Gabazine (10 μM) was added in the bath to block GABA$_A$ receptors. Whole-cell current clamp recordings were obtained from dSPNs or iSPNs in the dorsolateral striatum identified by their fluorescence. Patch pipettes (3–4 MΩ resistance) were loaded with internal solution containing (mM): 115 K-gluconate, 20 KCl, 1.5 MgCl$_2$, 5 HEPES, 0.2 EGTA, 2 Mg-ATP, 0.5 Na-GTP, 10 Na-phosphocreatine (pH 7.25, osmolarity 280–290 mOsm/l). The only exception was Mg$^{2+}$-free LTP experiments in which ACSF contained nominal zero Mg$^{2+}$ and Mg-ATP in pipette solution was replaced by Na-ATP. All the recordings were made using a MultiClamp 700B amplifier (Axon Instrument, USA), and signals were filtered at 2 kHz and digitized at 10 kHz. Stimulation and data acquisition were performed with PraireView5.

Corticostriatal EPSPs (2–8 mV) were evoked by a parallel bipolar electrode (0.2 ms) placed in deeper layers of the cortex. To assess synaptic summation, a train of five stimuli (40 Hz) was delivered every 20 s. To assess somatic excitability, gabazine was omitted from ACSF. Currents of increasing amplitudes (20–300 pA, 500 ms) were injected, and the number of evoked somatic action potentials was measured. To induce LTP in normal ACSF, HFS (100 Hz for 1 s) was paired with current injection (1–2 nA, 1 s), which was repeated four times with 20 s intervals. To induce LTP in Mg$^{2+}$-free condition, Mg$^{2+}$ was omitted from ACSF and pipette solution, and LTP was induced in dSPNs by three trains of HFS (100 Hz for 1 s) with 20-s intervals (Calabresi et al., 1992a).

Data analysis was conducted with custom scripts written in Python 3 (available upon request) and Prism 6. Non-parametric Wilcoxon or Mann-Whitney tests were used, and a *P* value less than 0.05 was considered statistically significant.

### 4.23. Stereotaxic viral injection

Wildtype and CDGI knockout mice (8–12 weeks old, male) were anesthetized using an isoflurane precision vaporizer (Kent Scientific, at 5% isoflurane during induction and 2% isoflurane during maintenance phase) and positioned in a stereotaxic frame (David Kopf Instruments, Tujunga, CA). Mice were administered with analgesics meloxicam (METACAM®, 0.1 mg/kg, s.c., Covetrus) before surgery. After the skin and fascia were retracted to reveal the skull, a small hole was drilled, and an injection needle was slowly inserted into the striatum. The viral vector (AAV9-hSyn-iAChSnFR, 800 nl, titer: 8–10 × 10$^{12}$, a generous gift of Looger lab (Borden et al., 2020)) was slowly infused at the following coordinates (in mm): AP 1, ML ±2 and DV −3 relative to Bregma. The injection needle was left in place for 5 min to allow tissue absorption of the virus, and then withdrawn. The mice were then sutured and placed on a heating pad until recovery from anesthesia. Imaging experiments were performed 3–5 weeks after viral injection.

### 4.24. Two-photon laser-scanning microscopy (2PLSM)

ACh release was assessed by imaging iAChSnFR (Borden et al., 2020), a genetically encoded fluorescent sensor of ACh (pAAV.hSynap. iAChSnFR was a gift from Loren Looger (Addgene plasmid #137950; http://n2t.net/addgene:137950; RRID: Addgene_137,950)), using 2PLSM. Acute parasagittal slices with striatal expression of iAChSnFR were prepared as described above, transferred to a recording chamber, and continuously perfused with normal ACSF at 32–34 °C. A two-photon laser (Chameleon Ultra II, Coherent, Santa Clara, CA) tuned to 920 nm was used to excite iAChSnFR. Fluorescence was imaged using an Ultima Laser Scanning Microscope system (Bruker, Billerica, MA) with an Olympus 60×/0.9 NA water-immersion objective lens and a Hamamatsu H7422P-40 GaAsP PMT (490 nm to 560 nm, Hamamatsu Photonics, Hamamatsu, Japan). Time series images of iAChSnFR were acquired with 0.388 μm × 0.388 μm pixels, 4-μs dwell time and a frame rate of 2.754 fps. After 30-s baseline acquisition, synchronous ACh release was evoked by delivering a train of 20 electrical stimuli (1 ms × 50 μA, at 2 Hz and 20 Hz) by a concentric bipolar electrode (FHC, Bowdoin, ME) placed at 200 μm ventral to the region of interest. Imaging was continued for at least another minute. Two trials were performed for each stimulation protocol. The dynamic range of the optical probe was determined by applying 10 μM cadmium chloride (to block any basal transmission) and 100 μM acetylcholine chloride (to saturate iAChSnFR signal) for determining minimal (Fmin) and maximal fluorescence intensity (Fmax). Because our preliminary data indicated that cadmium did not change basal fluorescence, we concluded that basal ACh level in acute slices is undetectable by iAChSnFR, and therefore cadmium chloride application was omitted. Fluorescent intensity data were analyzed by custom Python code (available upon request). Briefly, the fluorescence intensity values were first background-subtracted (the background resulted from PMT was measured by imaging with same PMT voltage but zero laser power) and averaged over two trials. Baseline fluorescence F$_0$ was the mean fluorescence over the 10 s right before stimulation and ΔF/(Fmax − Fmin) was quantified and presented.

### 4.25. Confocal microscopy of CDGI knockouts crossed to transgenic reporter lines

Anesthetized CDGI knockout mice crossed with reporter lines (D1-tdTomato x CDGI knockouts or D2-EGFP x CDGI knockouts) were perfused transcardially with saline briefly (~1 min) and then with ice-cold 4% paraformaldehyde (wt/vol) in 1× phosphate buffered saline (4% PFA-PBS). Brains were dissected out and incubated in 4% PFA-PBS overnight at 4 °C. Sagittal slices (100-μm thick) were cut using a Leica vibratome (VT1200S, Leica Biosystems, Wetzlar, Germany), mounted with Vectashield (Vector Laboratories), and viewed under a laser scanning confocal microscope (FV10i; Olympus). Images were adjusted for brightness, contrast and pseudo-coloring in ImageJ (US National Institutes of Health).

Supplementary data to this article can be found online at https://doi.org/10.1016/j.nbd.2021.105473.

## Acknowledgments

## References

Albin, R.L., Young, A.B., Penney, J.B., 1989. The functional anatomy of basal ganglia disorders. Trends Neurosci. 12 (10), 366–375. https://doi.org/10.1016/0166-2236(89)90074-x.

Alcacer, C., Andreoli, L., Sebastianutto, I., Jakobsson, J., Fieblinger, T., Cenci, M.A., 2017. Chemogenetic stimulation of striatal projection neurons modulates responses to Parkinson's disease therapy. J. Clin. Invest. 127 (2), 720–734. https://doi.org/10.1172/JCI90132.

Aliane, V., Perez, S., Bohren, Y., Deniau, J.M., Kemel, M.L., 2011. Key role of striatal cholinergic interneurons in processes leading to arrest of motor stereotypies. Brain 134 (Pt 1), 110–118. https://doi.org/10.1093/brain/awq285.

Augustin, S.M., Chancey, J.H., Lovinger, D.M., 2018. Dual dopaminergic regulation of corticostriatal plasticity by cholinergic interneurons and indirect pathway medium spiny neurons. Cell Rep. 24 (11), 2883–2893. https://doi.org/10.1016/j.celrep.2018.08.042.

Barnes, T.D., Kubota, Y., Hu, D., Jin, D.Z., Graybiel, A.M., 2005. Activity of striatal neurons reflects dynamic encoding and recoding of procedural memories. Nature 437 (7062), 1158–1161. https://doi.org/10.1038/nature04053.

Bernard, V., Normand, E., Bloch, B., 1992. Phenotypical characterization of the rat striatal neurons expressing muscarinic receptor genes. J. Neurosci. 12 (9), 3591–3600. https://www.ncbi.nlm.nih.gov/pubmed/1527598.

Borden, P.M., Zhang, P., Shivange, A.V., Marvin, J.S., Cichon, J., Dan, C., Podgorski, K., Figueiredo, A., Novak, O., Tanimoto, M., Shigetomi, E., Lobas, M.A., Kim, H., Zhu, P. K., Zhang, Y., Zheng, W.S., Fan, C., Wang, G., Xiang, B., Gan, L., Zhang, G.-X., Guo, K., Lin, L., Cai, Y., Yee, A.G., Aggarwal, A., Ford, C.P., Rees, D.C., Dietrich, D., Khakh, B.S., Dittman, J.S., Gan, W.-B., Koyama, M., Jayaraman, V., Cheer, J.F., Lester, H.A., Zhu, J.J., Looger, L.L., 2020. A fast genetically encoded fluorescent sensor for faithful in vivo acetylcholine detection in mice, fish, worms and flies. bioRxiv. https://doi.org/10.1101/2020.02.07.939504, 2020.2002.2007.939504.

Boyer, S.B., Slesinger, P.A., Jones, S.V., 2009. Regulation of Kir2.1 channels by the rho-GTPase, Rac1. J. Cell. Physiol. 218 (2), 385–393. https://doi.org/10.1002/jcp.21610.

Bradfield, L.A., Bertran-Gonzalez, J., Chieng, B., Balleine, B.W., 2013. The thalamostriatal pathway and cholinergic control of goal-directed action: interlacing new with existing learning in the striatum. Neuron 79 (1), 153–166. https://doi.org/10.1016/j.neuron.2013.04.039.

Brasted, P.J., Humby, T., Dunnett, S.B., Robbins, T.W., 1997. Unilateral lesions of the dorsal striatum in rats disrupt responding in egocentric space. J. Neurosci. 17 (22), 8919–8926. https://www.ncbi.nlm.nih.gov/pubmed/9348358.

Braun, A.A., Graham, D.L., Schaefer, T.L., Vorhees, C.V., Williams, M.T., 2012. Dorsal striatal dopamine depletion impairs both allocentric and egocentric navigation in rats. Neurobiol. Learn. Mem. 97 (4), 402–408. https://doi.org/10.1016/j.nlm.2012.03.004.

Calabresi, P., Maj, R., Pisani, A., Mercuri, N.B., Bernardi, G., 1992a. Long-term synaptic depression in the striatum: physiological and pharmacological characterization. J. Neurosci. 12 (11), 4224–4233. https://www.ncbi.nlm.nih.gov/pubmed/1359031.

Calabresi, P., Pisani, A., Mercuri, N.B., Bernardi, G., 1992b. Long-term potentiation in the striatum is unmasked by removing the voltage-dependent magnesium block of NMDA receptor channels. Eur. J. Neurosci. 4 (10), 929–935. https://doi.org/10.1111/j.1460-9568.1992.tb00119.x.

Calabresi, P., Centonze, D., Gubellini, P., Bernardi, G., 1999. Activation of M1-like muscarinic receptors is required for the induction of corticostriatal LTP. Neuropharmacology 38 (2), 323–326. https://doi.org/10.1016/s0028-3908(98)00199-3.

Canault, M., Ghalloussi, D., Grosdidier, C., Guinier, M., Perret, C., Chelghoum, N., Germain, M., Raslova, H., Peiretti, F., Morange, P.E., Saut, N., Pillois, X., Nurden, A.

T., Cambien, F., Pierres, A., van den Berg, T.K., Kuijpers, T.W., Alessi, M.C., Tregouet, D.A., 2014. Human CalDAG-GEFI gene (RASGRP2) mutation affects platelet function and causes severe bleeding. J. Exp. Med. 211 (7), 1349–1362. https://doi.org/10.1084/jem.20130477.

Cantuti-Castelvetri, I., Klucken, J., Ingelsson, M., Ramasamy, K., McLean, P.J., Frosch, M. P., Hyman, B.T., Standaert, D.G., 2005. Alpha-synuclein and chaperones in dementia with Lewy bodies. J. Neuropathol. Exp. Neurol. 64 (12), 1058–1066. https://www.ncbi.nlm.nih.gov/pubmed/16319716.

Carrillo-Reid, L., Day, M., Xie, Z., Melendez, A.E., Kondapalli, J., Plotkin, J.L., Wokosin, D.L., Chen, Y., Kress, G.J., Kaplitt, M., Ilijic, E., Guzman, J.N., Chan, C.S., Surmeier, D.J., 2019. Mutant huntingtin enhances activation of dendritic Kv4 K(+) channels in striatal spiny projection neurons. Elife 8. https://doi.org/10.7554/eLife.40818.

Choy, K.H., Shackleford, D.M., Malone, D.T., Mistry, S.N., Patil, R.T., Scammells, P.J., Langmead, C.J., Pantelis, C., Sexton, P.M., Lane, J.R., Christopoulos, A., 2016. Positive allosteric modulation of the muscarinic M1 receptor improves efficacy of antipsychotics in mouse glutamatergic deficit models of behavior. J. Pharmacol. Exp. Ther. 359 (2), 354–365. https://doi.org/10.1124/jpet.116.235788.

Crawley, J.N., 2000. What's Wrong with my Mouse? : Behavioral Phenotyping of Transgenic and Knockout Mice. Wiley-Liss.

Crittenden, J.R., Graybiel, A.M., 2016. Disease-associated changes in the striosome and matrix compartments of the dorsal striatum. In: Steiner, H., Tseng, K.Y. (Eds.), Handbook of behavioral neuroscience, vol. 24. Elsevier, pp. 783–802. https://doi.org/10.1016/B978-0-12-802206-1.00039-8.

Crittenden, J.R., Bergmeier, W., Zhang, Y., Piffath, C.L., Liang, Y., Wagner, D.D., Housman, D.E., Graybiel, A.M., 2004. CalDAG-GEFI integrates signaling for platelet aggregation and thrombus formation. Nat. Med. 10 (9), 982–986. https://doi.org/10.1038/nm1098.

Crittenden, J.R., Cantuti-Castelvetri, I., Saka, E., Keller-McGandy, C.E., Hernandez, L.F., Kett, L.R., Young, A.B., Standaert, D.G., Graybiel, A.M., 2009. Dysregulation of CalDAG-GEFI and CalDAG-GEFII predicts the severity of motor side-effects induced by anti-parkinsonian therapy. Proc. Natl. Acad. Sci. U. S. A. 106 (8), 2892–2896. https://doi.org/10.1073/pnas.0812822106.

Crittenden, J.R., Dunn, D.E., Merali, F.I., Woodman, B., Yim, M., Borkowska, A.E., Frosch, M.P., Bates, G.P., Housman, D.E., Lo, D.C., Graybiel, A.M., 2010. CalDAG-GEFI down-regulation in the striatum as a neuroprotective change in Huntington's disease. Hum. Mol. Genet. 19 (9), 1756–1765. https://doi.org/10.1093/hmg/ddq055.

Crittenden, J.R., Lacey, C.J., Lee, T., Bowden, H.A., Graybiel, A.M., 2014. Severe drug-induced repetitive behaviors and striatal overexpression of VAChT in ChAT-ChR2-EYFP BAC transgenic mice. Front. Neural. Circuits. 8, 57. https://doi.org/10.3389/fncir.2014.00057.

Crittenden, J.R., Tillberg, P.W., Riad, M.H., Shima, Y., Gerfen, C.R., Curry, J., Housman, D.E., Nelson, S.B., Boyden, E.S., Graybiel, A.M., 2016. Striosome-dendron bouquets highlight a unique striatonigral circuit targeting dopamine-containing neurons. Proc. Natl. Acad. Sci. U. S. A. 113 (40), 11318–11323. https://doi.org/10.1073/pnas.1613337113.

Crittenden, J.R., Sauvage, M., Kitsukawa, T., Burguière, E., Cepeda, C., André, V.M., Canault, M., Thomsen, M., Zhang, H., Costa, C., Martella, G., Ghiglieri, V., Pescatore, K.A., Unterwald, E.M., Jackson, W., Housman, D.E., Caine, S.B., Sulzer, D., Calabresi, P., Levine, M.S., Brefel-Courbon, C., Smith, A.C., Alessi, M.-C., Azulay, J.-P., Graybiel, A.M., 2019. Mutations in CalDAG-GEFI lead to striatal signaling deficits and psychomotor symptoms in multiple species including human. bioRxiv 709246. https://doi.org/10.1101/709246.

Crittenden, J.R., Yoshida, T., Davis, M.I., Graybiel, A.M., 2021. Immunofluorescence for free-floating brain sections. Protocols.io. https://doi.org/10.17504/protocols.io.kracv2e.

Dautan, D.H.-O., Witten, I., Deisseroth, K., Bolam, J.P., Gerdjikov, T., Mena-Segovia, J., 2014. A major external source of cholinergic innervation of the striatum and nucleus accumbens originates in the brainstem. J. Neurosci. 34 (13), 4509–4518. http://www.jneurosci.org/content/34/13/4509.full.pdf.

Dautan, D., Huerta-Ocampo, I., Gut, N.K., Valencia, M., Kondabolu, K., Kim, Y., Gerdjikov, T.V., Mena-Segovia, J., 2020. Cholinergic midbrain afferents modulate striatal circuits and shape encoding of action strategies. Nat. Commun. 11 (1), 1739. https://doi.org/10.1038/s41467-020-15514-3.

Day, M., Wokosin, D., Plotkin, J.L., Tian, X., Surmeier, D.J., 2008. Differential excitability and modulation of striatal medium spiny neuron dendrites. J. Neurosci. 28 (45), 11603–11614. https://doi.org/10.1523/JNEUROSCI.1840-08.2008.

DeLong, M.R., 1990. Primate models of movement disorders of basal ganglia origin. Trends Neurosci. 13 (7), 281–285. https://doi.org/10.1016/0166-2236(90)90110-v.

Desplats, P.A., Kass, K.E., Gilmartin, T., Stanwood, G.D., Woodward, E.L., Head, S.R., Sutcliffe, J.G., Thomas, E.A., 2006. Selective deficits in the expression of striatal-enriched mRNAs in Huntington's disease. J. Neurochem. 96 (3), 743–757. https://doi.org/10.1111/j.1471-4159.2005.03588.x.

Evans, R.C., Twedell, E.L., Zhu, M., Ascencio, J., Zhang, R., Khaliq, Z.M., 2020. Functional dissection of basal ganglia inhibitory inputs onto substantia nigra dopaminergic neurons. Cell Rep. 32 (11), 108156. https://doi.org/10.1016/j.celrep.2020.108156.

Fabbrini, G., Brotchie, J.M., Grandas, F., Nomoto, M., Goetz, C.G., 2007. Levodopa-induced dyskinesias. Mov. Disord. 22 (10), 1379–1389 quiz 1523. https://doi.org/10.1002/mds.21475.

Farrar, A.M., Callahan, J.W., Abercrombie, E.D., 2011. Reduced striatal acetylcholine efflux in the R6/2 mouse model of Huntington's disease: an examination of the role of altered inhibitory and excitatory mechanisms. Exp. Neurol. 232 (2), 119–125. https://doi.org/10.1016/j.expneurol.2011.08.010.

Gerber, D.J., Sotnikova, T.D., Gainetdinov, R.R., Huang, S.Y., Caron, M.G., Tonegawa, S., 2001. Hyperactivity, elevated dopaminergic transmission, and response to amphetamine in M1 muscarinic acetylcholine receptor-deficient mice. Proc. Natl. Acad. Sci. U. S. A. 98 (26), 15312–15317. https://doi.org/10.1073/pnas.261583798.

Gerdeman, G.L., Ronesi, J., Lovinger, D.M., 2002. Postsynaptic endocannabinoid release is critical to long-term depression in the striatum. Nat. Neurosci. 5 (5), 446–451. https://doi.org/10.1038/nn832.

Gerfen, C.R., Surmeier, D.J., 2011. Modulation of striatal projection systems by dopamine. Annu. Rev. Neurosci. 34, 441–466. https://doi.org/10.1146/annurev-neuro-061010-113641.

Gertler, T.S., Chan, C.S., Surmeier, D.J., 2008. Dichotomous anatomical properties of adult striatal medium spiny neurons. J. Neurosci. 28 (43), 10814–10824. https://doi.org/10.1523/JNEUROSCI.2660-08.2008.

Gong, S., Zheng, C., Doughty, M.L., Losos, K., Didkovsky, N., Schambra, U.B., Nowak, N. J., Joyner, A., Leblanc, G., Hatten, M.E., Heintz, N., 2003. A gene expression atlas of the central nervous system based on bacterial artificial chromosomes. Nature 425 (6961), 917–925. https://doi.org/10.1038/nature02033.

Graybiel, A.M., 1998. The basal ganglia and chunking of action repertoires. Neurobiol. Learn. Mem. 70 (1–2), 119–136. https://doi.org/10.1006/nlme.1998.3843.

Graybiel, A.M., 2008. Habits, rituals, and the evaluative brain. Annu. Rev. Neurosci. 359-387 https://doi.org/10.1146/annurev.neuro.29.051605.112851.

Graybiel, A.M., Grafton, S.T., 2015. The striatum: where skills and habits meet. Cold Spring Harb. Perspect. Biol. 7 (8), a021691. https://doi.org/10.1101/cshperspect.a021691.

Graybiel, A.M., Ragsdale Jr., C.W., 1978. Histochemically distinct compartments in the striatum of human, monkeys, and cat demonstrated by acetylthiocholinesterase staining. Proc. Natl. Acad. Sci. U. S. A. 75 (11), 5723–5726. http://www.ncbi.nlm.nih.gov/pubmed/103101.

Graybiel, A.M., Baughman, R.W., Eckenstein, F., 1986. Cholinergic neuropil of the striatum observes striosomal boundaries. Nature 323 (6089), 625–627. https://doi.org/10.1038/323625a0.

Graybiel, A.M., Canales, J.J., Capper-Loup, C., 2000. Levodopa-induced dyskinesias and dopamine-dependent stereotypies: a new hypothesis. Trends Neurosci. 23 (10 Suppl), S71–S77. https://doi.org/10.1016/s1471-1931(00)00027-6.

Guitart-Masip, M., Johansson, B., Fernandez-Teruel, A., Canete, T., Tobena, A., Terenius, L., Gimenez-Llort, L., 2006. Divergent anatomical pattern of D1 and D3 binding and dopamine- and cyclic AMP-regulated phosphoprotein of 32 kDa mRNA expression in the Roman rat strains: implications for drug addiction. Neuroscience 142 (4), 1231–1243. https://doi.org/10.1016/j.neuroscience.2006.07.041.

Guo, F.F., Kumahara, E., Saffen, D., 2001. A CalDAG-GEFI/Rap1/B-Raf cassette couples M(1) muscarinic acetylcholine receptors to the activation of ERK1/2. J. Biol. Chem. 276 (27), 25568–25581. https://doi.org/10.1074/jbc.M101277200.

Guru, S.C., Crabtree, J.S., Brown, K.D., Dunn, K.J., Manickam, P., Prasad, N.B., Wangsa, D., Burns, A.L., Spiegel, A.M., Marx, S.J., Pavan, W.J., Collins, F.S., Chandrasekharappa, S.C., 1999. Isolation, genomic organization, and expression analysis of Men1, the murine homolog of the MEN1 gene. Mamm. Genome 10 (6), 592–596. http://www.ncbi.nlm.nih.gov/pubmed/10341092.

Hansen, S.B., Tao, X., MacKinnon, R., 2011. Structural basis of PIP2 activation of the classical inward rectifier K+ channel Kir2.2. Nature 477 (7365), 495–498. https://doi.org/10.1038/nature10370.

Heinsbroek, J.A., Neuhofer, D.N., Griffin 3rd, W.C., Siegel, G.S., Bobadilla, A.C., Kupchik, Y.M., Kalivas, P.W., 2017. Loss of plasticity in the D2-accumbens pallidal pathway promotes cocaine seeking. J. Neurosci. 37 (4), 757–767. https://doi.org/10.1523/JNEUROSCI.2659-16.2016.

Hernandez-Flores, T., Hernandez-Gonzalez, O., Perez-Ramirez, M.B., Lara-Gonzalez, E., Arias-Garcia, M.A., Duhne, M., Perez-Burgos, A., Prieto, G.A., Figueroa, A., Galarraga, E., Bargas, J., 2015. Modulation of direct pathway striatal projection neurons by muscarinic M(4)-type receptors. Neuropharmacology 89, 232–244. https://doi.org/10.1016/j.neuropharm.2014.09.028.

Hersch, S.M., Gutekunst, C.A., Rees, H.D., Heilman, C.J., Levey, A.I., 1994. Distribution of m1-m4 muscarinic receptor proteins in the rat striatum: light and electron microscopic immunocytochemistry using subtype-specific antibodies. J. Neurosci. 14 (5 Pt 2), 3351–3363. https://www.ncbi.nlm.nih.gov/pubmed/8182478.

Huang, C.C., You, J.L., Wu, M.Y., Hsu, K.S., 2004. Rap1-induced p38 mitogen-activated protein kinase activation facilitates AMPA receptor trafficking via the GDI.Rab5 complex. Potential role in (S)-3,5-dihydroxyphenylglycene-induced long term depression. J. Biol. Chem. 279 (13), 12286–12292. https://doi.org/10.1074/jbc.M312868200.

Impey, S., Obrietan, K., Storm, D.R., 1999. Making new connections: role of ERK/MAP kinase signaling in neuronal plasticity. Neuron 23 (1), 11–14. https://doi.org/10.1016/s0896-6273(00)80747-3.

Janickova, H., Prado, V.F., Prado, M.A.M., El Mestikawy, S., Bernard, V., 2017. Vesicular acetylcholine transporter (VAChT) over-expression induces major modifications of striatal cholinergic interneuron morphology and function. J. Neurochem. 142 (6), 857–875. https://doi.org/10.1111/jnc.14105.

Joseph, L., Thomsen, M., 2017. Effects of muscarinic receptor antagonists on cocaine discrimination in wild-type mice and in muscarinic receptor M1, M2, and M4 receptor knockout mice. Behav. Brain Res. 329, 75–83. https://doi.org/10.1016/j.bbr.2017.04.023.

Katzenschlager, R., Sampaio, C., Costa, J., Lees, A., 2003. Anticholinergics for symptomatic management of Parkinson's disease. Cochrane database Syst. Rev. (2), CD003735. https://doi.org/10.1002/14651858.CD003735.

Kawasaki, H., Springett, G.M., Toki, S., Canales, J.J., Harlan, P., Blumenstiel, J.P., Chen, E.J., Bany, I.A., Mochizuki, N., Ashbacher, A., Matsuda, M., Housman, D.E., Graybiel, A.M., 1998. A rap guanine nucleotide exchange factor enriched highly in the basal ganglia. Proc. Natl. Acad. Sci. U. S. A. 95 (22), 13278–13283. http://www.ncbi.nlm.nih.gov/pubmed/9789079.

Kincaid, A.E., Wilson, C.J., 1996. Corticostriatal innervation of the patch and matrix in the rat neostriatum. J. Comp. Neurol. 374 (4), 578–592. https://doi.org/10.1002/(SICI)1096-9861(19961028)374:4<578::AID-CNE7>3.0.CO;2-Z.

Kitagawa, G., Gersch, W., 1996. Smoothness Priors Analysis of Time Series. Springer.

Kitsukawa, T., Nagata, M., Yanagihara, D., Tomioka, R., Utsumi, H., Kubota, Y., Yagi, T., Graybiel, A.M., Yamamori, T., 2011. A novel instrumented multipeg running wheel system, step-wheel, for monitoring and controlling complex sequential stepping in mice. J. Neurophysiol. 106 (1), 479–487. https://doi.org/10.1152/jn.00139.2011.

Klaus, A., Alves da Silva, J., Costa, R.M., 2019. What, if, and when to move: basal ganglia circuits and self-paced action initiation. Annu. Rev. Neurosci. 42, 459–483. https://doi.org/10.1146/annurev-neuro-072116-031033.

Kosuru, R., Chrzanowska, M., 2020. Integration of Rap1 and calcium signaling. Int. J. Mol. Sci. 21 (5) https://doi.org/10.3390/ijms21051616.

Kreitzer, A.C., Malenka, R.C., 2005. Dopamine modulation of state-dependent endocannabinoid release and long-term depression in the striatum. J. Neurosci. 25 (45), 10537–10545. https://doi.org/10.1523/JNEUROSCI.2959-05.2005.

Kreitzer, A.C., Malenka, R.C., 2008. Striatal plasticity and basal ganglia circuit function. Neuron 60 (4), 543–554. https://doi.org/10.1016/j.neuron.2008.11.005.

Kuczenski, R., Segal, D.S., 1997. An escalating dose/multiple high-dose binge pattern of amphetamine administration results in differential changes in the extracellular dopamine response profiles in caudate-putamen and nucleus accumbens. J. Neurosci. 17 (11), 4441–4447. http://www.ncbi.nlm.nih.gov/pubmed/9151761.

Kuczenski, R., Segal, D.S., 2001. Caudate-putamen and nucleus accumbens extracellular acetylcholine responses to methamphetamine binges. Brain Res. 923 (1–2), 32–38. http://www.ncbi.nlm.nih.gov/pubmed/11743969.

Kuhn, A., Goldstein, D.R., Hodges, A., Strand, A.D., Sengstag, T., Kooperberg, C., Becanovic, K., Pouladi, M.A., Sathasivam, K., Cha, J.H., Hannan, A.J., Hayden, M.R., Leavitt, B.R., Dunnett, S.B., Ferrante, R.J., Albin, R., Shelbourne, P., Delorenzi, M., Augood, S.J., Faull, R.L., Olson, J.M., Bates, G.P., Jones, L., Luthi-Carter, R., 2007. Mutant huntingtin's effects on striatal gene expression in mice recapitulate changes observed in human Huntington's disease brain and do not differ with mutant huntingtin length or wild-type huntingtin dosage. Hum. Mol. Genet. 16 (15), 1845–1861. https://doi.org/10.1093/hmg/ddm133.

Lebois, E.P., Bridges, T.M., Lewis, L.M., Dawson, E.S., Kane, A.S., Xiang, Z., Jadhav, S.B., Yin, H., Kennedy, J.P., Meiler, J., Niswender, C.M., Jones, C.K., Conn, P.J., Weaver, C.D., Lindsley, C.W., 2010. Discovery and characterization of novel subtype-selective allosteric agonists for the investigation of M(1) receptor function in the central nervous system. ACS Chem. Neurosci. 1 (2), 104–121. https://doi.org/10.1021/cn900003h.

Lemberger, T., Parlato, R., Dassesse, D., Westphal, M., Casanova, E., Turiault, M., Tronche, F., Schiffmann, S.N., Schutz, G., 2007. Expression of Cre recombinase in dopaminoceptive neuron. BMC Neurosci. 8, 4. https://doi.org/10.1186/1471-2202-8-4.

Luthi-Carter, R., Hanson, S.A., Strand, A.D., Bergstrom, D.A., Chun, W., Peters, N.L., Woods, A.M., Chan, E.Y., Kooperberg, C., Krainc, D., Young, A.B., Tapscott, S.J., Olson, J.M., 2002. Dysregulation of gene expression in the R6/2 model of polyglutamine disease: parallel changes in muscle and brain. Hum. Mol. Genet. 11 (17), 1911–1926. https://doi.org/10.1093/hmg/11.17.1911.

Lv, X., Dickerson, J.W., Rook, J.M., Lindsley, C.W., Conn, P.J., Xiang, Z., 2017. M1 muscarinic activation induces long-lasting increase in intrinsic excitability of striatal projection neurons. Neuropharmacology 118, 209–222. https://doi.org/10.1016/j.neuropharm.2017.03.017.

Martiros, N., Burgess, A.A., Graybiel, A.M., 2018. Inversely active striatal projection neurons and interneurons selectively delimit useful behavioral sequences. Curr. Biol. 28 (4), 560–573 e565. https://doi.org/10.1016/j.cub.2018.01.031.

McCool, M.F., Patel, S., Talati, R., Ragozzino, M.E., 2008. Differential involvement of M1-type and M4-type muscarinic cholinergic receptors in the dorsomedial striatum in task switching. Neurobiol. Learn. Mem. 89 (2), 114–124. https://doi.org/10.1016/j.nlm.2007.06.005.

McGregor, M.M., McKinsey, G.L., Girasole, A.E., Bair-Marshall, C.J., Rubenstein, J.L.R., Nelson, A.B., 2019. Functionally distinct connectivity of developmentally targeted Striosome neurons. Cell Rep. 29 (6), 1419–1428 e1415. https://doi.org/10.1016/j.celrep.2019.09.076.

Mink, J.W., 1996. The basal ganglia: focused selection and inhibition of competing motor programs. Prog. Neurobiol. 50 (4), 381–425. https://doi.org/10.1016/s0301-0082(96)00042-1.

Monory, K., Blaudzun, H., Massa, F., Kaiser, N., Lemberger, T., Schutz, G., Wotjak, C.T., Lutz, B., Marsicano, G., 2007. Genetic dissection of behavioural and autonomic effects of Delta(9)-tetrahydrocannabinol in mice. PLoS Biol. 5 (10), e269 https://doi.org/10.1371/journal.pbio.0050269.

Moran, S.P., Maksymetz, J., Conn, P.J., 2019. Targeting muscarinic acetylcholine receptors for the treatment of psychiatric and neurological disorders. Trends Pharmacol. Sci. 40 (12), 1006–1020. https://doi.org/10.1016/j.tips.2019.10.007.

Moussa, R., Poucet, B., Amalric, M., Sargolini, F., 2011. Contributions of dorsal striatal subregions to spatial alternation behavior. Learn. Mem. 18 (7), 444–451. https://doi.org/10.1101/lm.2123811.

Nakamura, T., Nagata, M., Yagi, T., Graybiel, A.M., Yamamori, T., Kitsukawa, T., 2017. Learning new sequential stepping patterns requires striatal plasticity during the earliest phase of acquisition. Eur. J. Neurosci. 45 (7), 901–911. https://doi.org/10.1111/ejn.13537.

Narushima, M., Uchigashima, M., Fukaya, M., Matsui, M., Manabe, T., Hashimoto, K., Watanabe, M., Kano, M., 2007. Tonic enhancement of endocannabinoid-mediated retrograde suppression of inhibition by cholinergic interneuron activity in the

striatum. J. Neurosci. 27 (3), 496–506. https://doi.org/10.1523/JNEUROSCI.4644-06.2007.

Niemz, J., Kliche, S., Pils, M.C., Morrison, E., Manns, A., Freund, C., Crittenden, J.R., Graybiel, A.M., Galla, M., Jansch, L., Huehn, J., 2017. The guanine-nucleotide exchange factor CalDAG GEFI fine-tunes functional properties of regulatory T cells. Eur. J. Microbiol. Immunol. (Bp) 7 (2), 112–126. https://doi.org/10.1556/1886.2017.00007.

Oldenburg, I.A., Ding, J.B., 2011. Cholinergic modulation of synaptic integration and dendritic excitability in the striatum. Curr. Opin. Neurobiol. 21 (3), 425–432. https://doi.org/10.1016/j.conb.2011.04.004.

Packard, M.G., McGaugh, J.L., 1996. Inactivation of hippocampus or caudate nucleus with lidocaine differentially affects expression of place and response learning. Neurobiol. Learn. Mem. 65 (1), 65–72. https://doi.org/10.1006/nlme.1996.0007.

Panigrahi, B., Martin, K.A., Li, Y., Graves, A.R., Vollmer, A., Olson, L., Mensh, B.D., Karpova, A.Y., Dudman, J.T., 2015. Dopamine is required for the neural representation and control of movement vigor. Cell 162 (6), 1418–1430. https://doi.org/10.1016/j.cell.2015.08.014.

Paquet, M., Smith, Y., 2003. Group I metabotropic glutamate receptors in the monkey striatum: subsynaptic association with glutamatergic and dopaminergic afferents. J. Neurosci. 23 (20), 7659–7669. https://www.ncbi.nlm.nih.gov/pubmed/12930805.

Paxinos, G., Franklin, K., 2001. The Mouse Brain in Stereotaxic Coordinates. Academic Press.

Picconi, B., Centonze, D., Hakansson, K., Bernardi, G., Greengard, P., Fisone, G., Cenci, M.A., Calabresi, P., 2003. Loss of bidirectional striatal synaptic plasticity in L-DOPA-induced dyskinesia. Nat. Neurosci. 6 (5), 501–506. https://doi.org/10.1038/nn1040.

Pisani, A., Bernardi, G., Ding, J., Surmeier, D.J., 2007. Re-emergence of striatal cholinergic interneurons in movement disorders. Trends Neurosci. 30 (10), 545–553. https://doi.org/10.1016/j.tins.2007.07.008.

Plotkin, J.L., Surmeier, D.J., 2015. Corticostriatal synaptic adaptations in Huntington's disease. Curr. Opin. Neurobiol. 33, 53–62. https://doi.org/10.1016/j.conb.2015.01.020.

Plotkin, J.L., Day, M., Peterson, J.D., Xie, Z., Kress, G.J., Rafalovich, I., Kondapalli, J., Gertler, T.S., Flajolet, M., Greengard, P., Stavarache, M., Kaplitt, M.G., Rosinski, J., Chan, C.S., Surmeier, D.J., 2014. Impaired TrkB receptor signaling underlies corticostriatal dysfunction in Huntington's disease. Neuron 83 (1), 178–188. https://doi.org/10.1016/j.neuron.2014.05.032.

Rhee, S.G., 2001. Regulation of phosphoinositide-specific phospholipase C. Annu. Rev. Biochem. 70, 281–312. https://doi.org/10.1146/annurev.biochem.70.1.281.

Rogers, D.C., Fisher, E.M., Brown, S.D., Peters, J., Hunter, A.J., Martin, J.E., 1997. Behavioral and functional analysis of mouse phenotype: SHIRPA, a proposed protocol for comprehensive phenotype assessment. Mamm. Genome 8 (10), 711–713. http://www.ncbi.nlm.nih.gov/pubmed/9321461.

Saka, E., Iadarola, M., Fitzgerald, D.J., Graybiel, A.M., 2002. Local circuit neurons in the striatum regulate neural and behavioral responses to dopaminergic stimulation. Proc. Natl. Acad. Sci. U. S. A. 99 (13), 9004–9009. https://doi.org/10.1073/pnas.132212499.

Saka, E., Goodrich, C., Harlan, P., Madras, B.K., Graybiel, A.M., 2004. Repetitive behaviors in monkeys are linked to specific striatal activation patterns. J. Neurosci. 24 (34), 7557–7565. https://doi.org/10.1523/JNEUROSCI.1072-04.2004.

Sarker, M., Goliaei, A., Golesi, F., Poggi, M., Cook, A.A., Khan, M.A.I., Temple, B.R., Stefanini, L., Canault, M., Bergmeier, W., Campbell, S.L., 2020. Subcellular localization of Rap1 GTPase activator CalDAG-GEFI is orchestrated by interaction of its atypical C1 domain with membrane phosphoinositides. J. Thromb. Haemost. 18 (3), 693–705. https://doi.org/10.1111/jth.14687.

Schreiweis, C., Bornschein, U., Burguiere, E., Kerimoglu, C., Schreiter, S., Dannemann, M., Goyal, S., Rea, E., French, C.A., Puliyadi, R., Groszer, M., Fisher, S. E., Mundry, R., Winter, C., Hevers, W., Paabo, S., Enard, W., Graybiel, A.M., 2014. Humanized Foxp2 accelerates learning by enhancing transitions from declarative to procedural performance. Proc. Natl. Acad. Sci. U. S. A. 111 (39), 14253–14258. https://doi.org/10.1073/pnas.1414542111.

Schultz, W., 2019. Recent advances in understanding the role of phasic dopamine activity. F1000Res 8. https://doi.org/10.12688/f1000research.19793.1.

Sheffler, D.J., Williams, R., Bridges, T.M., Xiang, Z., Kane, A.S., Byun, N.E., Jadhav, S., Mock, M.M., Zheng, F., Lewis, L.M., Jones, C.K., Niswender, C.M., Weaver, C.D., Lindsley, C.W., Conn, P.J., 2009. A novel selective muscarinic acetylcholine receptor subtype 1 antagonist reduces seizures without impairing hippocampus-dependent learning. Mol. Pharmacol. 76 (2), 356–368. https://doi.org/10.1124/mol.109.056531.

Shen, W., Hamilton, S.E., Nathanson, N.M., Surmeier, D.J., 2005. Cholinergic suppression of KCNQ channel currents enhances excitability of striatal medium spiny neurons. J. Neurosci. 25 (32), 7449–7458. https://doi.org/10.1523/JNEUROSCI.1381-05.2005.

Shen, W., Tian, X., Day, M., Ulrich, S., Tkatch, T., Nathanson, N.M., Surmeier, D.J., 2007. Cholinergic modulation of Kir2 channels selectively elevates dendritic excitability in striatopallidal neurons. Nat. Neurosci. 10 (11), 1458–1466. https://doi.org/10.1038/nn1972.

Shen, W., Flajolet, M., Greengard, P., Surmeier, D.J., 2008. Dichotomous dopaminergic control of striatal synaptic plasticity. Science 321 (5890), 848–851. https://doi.org/10.1126/science.1160575.

Shen, W., Plotkin, J.L., Francardo, V., Ko, W.K., Xie, Z., Li, Q., Fieblinger, T., Wess, J., Neubig, R.R., Lindsley, C.W., Conn, P.J., Greengard, P., Bezard, E., Cenci, M.A., Surmeier, D.J., 2015. M4 muscarinic receptor signaling ameliorates striatal plasticity deficits in models of L-DOPA-induced dyskinesia. Neuron 88 (4), 762–773. https://doi.org/10.1016/j.neuron.2015.10.039.

Shen, W., Ren, W., Zhai, S., Yang, B., Vanoye, C.G., Mitra, A., George Jr., A.L., Surmeier, D.J., 2020. Striatal Kir2 K+ channel inhibition mediates the antidyskinetic effects of amantadine. J. Clin. Invest. 130 (5), 2593–2601. https://doi.org/10.1172/JCI133398.

Shin, J.H., Adrover, M.F., Wess, J., Alvarez, V.A., 2015. Muscarinic regulation of dopamine and glutamate transmission in the nucleus accumbens. Proc. Natl. Acad. Sci. U. S. A. 112 (26), 8124–8129. https://doi.org/10.1073/pnas.1508846112.

Smith, Y., Bolam, J.P., 1990. The output neurones and the dopaminergic neurones of the substantia nigra receive a GABA-containing input from the globus pallidus in the rat. J. Comp. Neurol. 296 (1), 47–64. https://doi.org/10.1002/cne.902960105.

Smith, A.C., Frank, L.M., Wirth, S., Yanike, M., Hu, D., Kubota, Y., Graybiel, A.M., Suzuki, W.A., Brown, E.N., 2004. Dynamic analysis of learning in behavioral experiments. J. Neurosci. 24 (2), 447–461. https://doi.org/10.1523/JNEUROSCI.2908-03.2004.

Soares, J.C., Oliveira, M.G., Ferreira, T.L., 2013. Inactivation of muscarinic receptors impairs place and response learning: implications for multiple memory systems. Neuropharmacology 73, 320–326. https://doi.org/10.1016/j.neuropharm.2013.06.009.

Steele, A.D., Jackson, W.S., King, O.D., Lindquist, S., 2007. The power of automated high-resolution behavior analysis revealed by its application to mouse models of Huntington's and prion diseases. Proc. Natl. Acad. Sci. U. S. A. 104 (6), 1983–1988. https://doi.org/10.1073/pnas.0610779104.

Stefanini, L., Bergmeier, W., 2010. CalDAG-GEFI and platelet activation. Platelets 21 (4), 239–243. https://doi.org/10.3109/09537101003639931.

Stefanini, L., Boulaftali, Y., Ouellette, T.D., Holinstat, M., Desire, L., Leblond, B., Andre, P., Conley, P.B., Bergmeier, W., 2012. Rap1-Rac1 circuits potentiate platelet activation. Arterioscler. Thromb. Vasc. Biol. 32 (2), 434–441. https://doi.org/10.1161/ATVBAHA.111.239194.

Stoll, K., Hart, R., Lindsley, C.W., Thomsen, M., 2018. Effects of muscarinic M1 and M4 acetylcholine receptor stimulation on extinction and reinstatement of cocaine seeking in male mice, independent of extinction learning. Psychopharmacology 235 (3), 815–827. https://doi.org/10.1007/s00213-017-4797-0.

Stoof, J.C., Kebabian, J.W., 1981. Opposing roles for D-1 and D-2 dopamine receptors in efflux of cyclic AMP from rat neostriatum. Nature 294 (5839), 366–368. https://doi.org/10.1038/294366a0.

Takeda, K., Ichijo, H., 2002. Neuronal p38 MAPK signalling: an emerging regulator of cell fate and function in the nervous system. Genes Cells 7 (11), 1099–1111. https://doi.org/10.1046/j.1365-2443.2002.00591.x.

Taverna, S., Ilijic, E., Surmeier, D.J., 2008. Recurrent collateral connections of striatal medium spiny neurons are disrupted in models of Parkinson's disease. J. Neurosci. 28 (21), 5504–5512. https://doi.org/10.1523/JNEUROSCI.5493-07.2008.

Thomas, A., Burant, A., Bui, N., Graham, D., Yuva-Paylor, L.A., Paylor, R., 2009. Marble burying reflects a repetitive and perseverative behavior more than novelty-induced anxiety. Psychopharmacology 204 (2), 361–373. https://doi.org/10.1007/s00213-009-1466-y.

Thomsen, M., Woldbye, D.P., Wortwein, G., Fink-Jensen, A., Wess, J., Caine, S.B., 2005. Reduced cocaine self-administration in muscarinic M5 acetylcholine receptor-deficient mice. J. Neurosci. 25 (36), 8141–8149. https://doi.org/10.1523/JNEUROSCI.2077-05.2005.

Thomsen, M., Conn, P.J., Lindsley, C., Wess, J., Boon, J.Y., Fulton, B.S., Fink-Jensen, A., Caine, S.B., 2010. Attenuation of cocaine's reinforcing and discriminative stimulus effects via muscarinic M1 acetylcholine receptor stimulation. J. Pharmacol. Exp. Ther. 332 (3), 959–969. https://doi.org/10.1124/jpet.109.162057.

Thomsen, M., Lindsley, C.W., Conn, P.J., Wessell, J.E., Fulton, B.S., Wess, J., Caine, S.B., 2012. Contribution of both M1 and M4 receptors to muscarinic agonist-mediated attenuation of the cocaine discriminative stimulus in mice. Psychopharmacology 220 (4), 673–685. https://doi.org/10.1007/s00213-011-2516-9.

Toki, S., Kawasaki, H., Tashiro, N., Housman, D.E., Graybiel, A.M., 2001. Guanine nucleotide exchange factors CalDAG-GEFI and CalDAG-GEFII are colocalized in striatal projection neurons. J. Comp. Neurol. 437 (4), 398–407. https://doi.org/10.1002/cne.1291.

Tzavos, A., Jih, J., Ragozzino, M.E., 2004. Differential effects of M1 muscarinic receptor blockade and nicotinic receptor blockade in the dorsomedial striatum on response reversal learning. Behav. Brain Res. 154 (1), 245–253. https://doi.org/10.1016/j.bbr.2004.02.011.

Unterwald, E.M., Ho, A., Rubenfeld, J.M., Kreek, M.J., 1994. Time course of the development of behavioral sensitization and dopamine receptor up-regulation during binge cocaine administration. J. Pharmacol. Exp. Ther. 270 (3), 1387–1396. https://www.ncbi.nlm.nih.gov/pubmed/7932193.

Unterwald, E.M., Kreek, M.J., Cuntapay, M., 2001. The frequency of cocaine administration impacts cocaine-induced receptor alterations. Brain Res. 900 (1), 103–109. http://www.ncbi.nlm.nih.gov/pubmed/11325352.

Wang, Z., Kai, L., Day, M., Ronesi, J., Yin, H.H., Ding, J., Tkatch, T., Lovinger, D.M., Surmeier, D.J., 2006. Dopaminergic control of corticostriatal long-term synaptic depression in medium spiny neurons is mediated by cholinergic interneurons. Neuron 50 (3), 443–452. https://doi.org/10.1016/j.neuron.2006.04.010.

Watabe-Uchida, M., Zhu, L., Ogawa, S.K., Vamanrao, A., Uchida, N., 2012. Whole-brain mapping of direct inputs to midbrain dopamine neurons. Neuron 74 (5), 858–873. https://doi.org/10.1016/j.neuron.2012.03.017.

Weikop, P., Jensen, K.L., Thomsen, M., 2020. Effects of muscarinic M1 receptor stimulation on reinforcing and neurochemical effects of cocaine in rats. Neuropsychopharmacology 45 (12), 1994–2002. https://doi.org/10.1038/s41386-020-0684-1.

Xu, M., Kobets, A., Du, J.C., Lennington, J., Li, L., Banasr, M., Duman, R.S., Vaccarino, F. M., DiLeone, R.J., Pittenger, C., 2015. Targeted ablation of cholinergic interneurons in the dorsolateral striatum produces behavioral manifestations of Tourette

syndrome. Proc. Natl. Acad. Sci. U. S. A. 112 (3), 893–898. https://doi.org/10.1073/pnas.1419533112.

Yan, Z., Flores-Hernandez, J., Surmeier, D.J., 2001. Coordinated expression of muscarinic receptor messenger RNAs in striatal medium spiny neurons. Neuroscience 103 (4), 1017–1024. https://doi.org/10.1016/s0306-4522(01)00039-2.

Yin, H.H., Knowlton, B.J., 2006. The role of the basal ganglia in habit formation. Nat. Rev. Neurosci. 7 (6), 464–476. https://doi.org/10.1038/nrn1919.

York, R.D., Yao, H., Dillon, T., Ellig, C.L., Eckert, S.P., McCleskey, E.W., Stork, P.J., 1998. Rap1 mediates sustained MAP kinase activation induced by nerve growth factor. Nature 392 (6676), 622–626. https://doi.org/10.1038/33451.

Zeitler, B., Froelich, S., Marlen, K., Shivak, D.A., Yu, Q., Li, D., Pearl, J.R., Miller, J.C., Zhang, L., Paschon, D.E., Hinkley, S.J., Ankoudinova, I., Lam, S., Guschin, D., Kopan, L., Cherone, J.M., Nguyen, H.B., Qiao, G., Ataei, Y., Mendel, M.C., Amora, R., Surosky, R., Laganiere, J., Vu, B.J., Narayanan, A., Sedaghat, Y., Tillack, K.,

Thiede, C., Gartner, A., Kwak, S., Bard, J., Mrzljak, L., Park, L., Heikkinen, T., Lehtimaki, K.K., Svedberg, M.M., Haggkvist, J., Tari, L., Toth, M., Varrone, A., Halldin, C., Kudwa, A.E., Ramboz, S., Day, M., Kondapalli, J., Surmeier, D.J., Urnov, F.D., Gregory, P.D., Rebar, E.J., Munoz-Sanjuan, I., Zhang, H.S., 2019. Allele-selective transcriptional repression of mutant HTT for the treatment of Huntington's disease. Nat. Med. 25 (7), 1131–1142. https://doi.org/10.1038/s41591-019-0478-3.

Zhai, S., Tanimura, A., Graves, S.M., Shen, W., Surmeier, D.J., 2018. Striatal synapses, circuits, and Parkinson's disease. Curr. Opin. Neurobiol. 48, 9–16. https://doi.org/10.1016/j.conb.2017.08.004.

Zhang, H., Sulzer, D., 2003. Glutamate spillover in the striatum depresses dopaminergic transmission by activating group I metabotropic glutamate receptors. J. Neurosci. 23 (33), 10585–10592. http://www.ncbi.nlm.nih.gov/pubmed/14627643.

Zhang, W., Yamada, M., Gomeza, J., Basile, A.S., Wess, J., 2002. Multiple muscarinic acetylcholine receptor subtypes modulate striatal dopamine release, as studied with M1-M5 muscarinic receptor knock-out mice. J. Neurosci. 22 (15), 6347–6352.